Raphael Kircher
Overhauser Dynamic Nuclear Polarization and Paragmagnetic Relaxation Enhancement in Continuous-Flow Benchtop NMR Spectroscopy
Scientific Report Series Volume 46
2024

Scientific Report Series
Laboratory of Engineering Thermodynamics (LTD)
TU Kaiserslautern
P.O. Box 3049
67663 Kaiserslautern
Germany

ISSN 2195-7606
ISBN 978-3-944433-45-5

Overhauser Dynamic Nuclear Polarization and Paramagnetic Relaxation Enhancement in Continuous-Flow Benchtop NMR Spectroscopy

Vom Fachbereich Maschinenbau und Verfahrenstechnik
der Technischen Universität Kaiserslautern
zur Verleihung des akademischen Grades

Doktor-Ingenieur (Dr.-Ing.)

genehmigte

Dissertation

von

Dipl.-Chem. Raphael Kircher
aus Speyer

Dekan:	Prof. Dr. rer. nat. Roland Ulber
Berichterstatter:	Prof. Dr.-Ing. Erik von Harbou
	Prof. Dr. Werner Thiel
	Prof. Dr.-Ing. Hans Hasse

Tag der mündlichen Prüfung: 16.02.2024

D 386

Danksagung

Die vorliegende Arbeit wurde während meiner Tätigkeit als wissenschaftlicher Mitarbeiter am Lehrstuhl für Thermodynamik (LTD) an der RPTU Kaiserslautern verfasst. An dieser Stelle möchte ich mich bei allen Personen bedanken, die mich während dieser Zeit unterstützt haben.

Ich möchte mich herzlich bei Prof. Dr.-Ing. Hans Hasse bedanken, der mir die Freiheit gegeben hat, mich in diesem Projekt zu entwickeln und mich in jeder Hinsicht unterstützt hat. Ein besonderer Dank gilt Prof. Dr.-Ing. Erik von Harbou, denn sein Engagement und seine Unterstützung haben maßgeblich dazu beigetragen, dass ich meine Leidenschaft als Wissenschaftler am LTD entwickeln konnte. Vielen Dank für die Übernahme des Vorsitzes der Prüfungskommission. Des Weiteren möchte ich Prof. Dr. Werner Thiel meinen Dank aussprechen, der mich bereits während meines Studiums in der Chemie unterstützt und im Schwerpunkt Katalyse gefördert hat. Vielen Dank für die Übernahme der Begutachtung dieser Arbeit. Die Unterstützung der Mitarbeiter am Lehrstuhl war für diese Arbeit von entscheidender Bedeutung. Ein besonderer Dank gilt dem Sekretariat, dem Labor-Team, sowie der IT des LTDs. Ihr ermöglicht das Arbeiten in einer wunderbaren Atmosphäre und tragt maßgeblich zum Erfolg bei. Auch den zahlreichen wissenschaftlichen Mitarbeitern danke ich für ihre Unterstützung und ihre wertvollen Beiträge. Viele Mitarbeiter des LTDs sind auch Freunde geworden, und ich schätze die tollen Momente, die wir bei der Arbeit, bei Betriebsausflügen, auf Konferenzen und in gemeinsamen Urlauben geteilt haben. Besonders möchte ich mich bei meiner Mentorin Dr. Kerstin Münnemann bedanken. Ihre Expertise und ihre Ermutigung waren für mich von großem Wert und haben zum Erfolg dieser Arbeit und meiner beruflichen Entwicklung beigetragen.

Abschließend möchte ich meiner Familie meinen tiefsten Dank aussprechen. Ohne euch wäre diese Arbeit nicht möglich gewesen. Vielen Dank für eure Liebe, euren Glauben an mich und die Unterstützung auf meinem Weg.

Kaiserslautern, March 2024

Raphael Kircher

Abstract

Nuclear magnetic resonance (NMR) spectroscopy is an excellent tool for reaction and process monitoring. Process monitoring is often carried out online on flowing samples. Benchtop NMR spectrometers are especially well-suited for these applications because they can be installed close to the studied process. However, it is a challenge to analyze a fast-flowing liquid with NMR spectroscopy because short residence times in the magnetic field of the spectrometer result in inefficient polarization build-up and thus poor signal intensity. This is particularly problematic for benchtop NMR spectrometers because of their compact design. Therefore, different methods to counteract this prepolarization problem in benchtop NMR spectroscopy were studied experimentally in the present work. Established approaches that were studied gave only poor results at high flow velocities. To overcome this, signal enhancement by Overhauser DNP (ODNP) was used, which is based on polarization transfer from unpaired electron spins to nuclear spins and happens on very short time scales, resulting in high signal enhancements, also in fast-flowing liquids. A corresponding set-up was developed and used for the studies: the line leading to the 1 Tesla benchtop NMR spectrometer first passes a fixed bed of a radical matrix which is placed in a Halbach magnet equipped with a microwave cavity to facilitate the polarization transfer. With this ODNP set-up, excellent results were obtained also for the highest studied flow velocities. This shows that ODNP is an enabler for fast-flow benchtop NMR spectroscopy.

ODNP requires the presence of unpaired electrons in the sample which is usually accomplished by addition of stable radicals. However, radicals affect the nuclear relaxation times and can hamper the NMR detection. This was circumvented by immobilizing radicals in a fixed bed, allowing for the measurement of radical-free samples when using ex-situ DNP techniques (DNP build-up and NMR detection happen at different places) with flow-induced separation of the hyperpolarized liquid from the radicals. Therefore, the synthesis of robust and chemically inert immobilized radical matrices is mandatory. This was accomplished by immobilizing the radical glycidyloxy-tetramethylpiperidinyloxyl (GT) with a polyethyleneimine (PEI) linker on the surface of controlled porous glasses (CPG). Both the porosity of the CPGs and also the size of the PEI-linker were varied resulting in a set of distinct radical matrices for continuous-flow ODNP. The study shows that CPGs with PEI-linkers provide robust, inert, and efficient ODNP matrices.

Another method to address the prepolarization problem in continuous-flow NMR applications is paramagnetic relaxation enhancement (PRE) by using a T_1 relaxation agent. In the present work, a PRE agent was developed that was again based on PEI-grafted CPGs with PEI-linker and GT. Here, the interaction of the studied liquid with this PRE agent significantly accelerates the buildup of nuclear polarization prior to NMR detection, which enables quantitative measurements in continuous-flow benchtop NMR applications. The results show that the flow regime for quantitative measurements can be greatly extended by the use of the synthesized PRE agent.

Kurzfassung

Die Kernspinresonanzspektroskopie (engl. Nuclear Magnetic Resonance: NMR) ist ein hervorragendes Instrument zur Reaktions- und Prozessüberwachung, welche häufig online an fließenden Proben durchgeführt wird. Benchtop-NMR Spektrometer sind für solche Anwendungen besonders gut geeignet, da diese Geräte in der Nähe des untersuchten Prozesses installiert werden können. Es ist jedoch generell eine Herausforderung, eine schnell fließende Flüssigkeit mit NMR-Spektroskopie zu analysieren, da kurze Verweilzeiten im Magnetfeld des Spektrometers zu einem ineffizienten Polarisationsaufbau und damit zu einer geringen Signalintensität führen. Dies ist speziell bei Benchtop-NMR Spektrometern, durch ihrer kompakte Bauweise, problematisch. In der vorliegenden Arbeit wurden verschiedene Methoden entwickelt, um diesem Vorpolarisationsproblem in der Benchtop-NMR Spektroskopie entgegenzuwirken. Zunächst wurde gezeigt, dass etablierte Ansätze schlechte Ergebnisse bei hohen Flussraten liefern. Um dieses Problem zu lösen, wurde einerseits die Signalverstärkung durch Overhauser DNP (ODNP) eingesetzt, welche auf der Polarisationsübertragung von ungepaarten Elektronenspins auf Kernspins beruht und auf sehr kurzen Zeitskalen abläuft, sodass auch in schnell fließenden Flüssigkeiten große Signalverbesserungen erzielt werden können. Ein entsprechender Aufbau wurde entwickelt. Dabei führt die Leitung mit der fließenden Probe zunächst durch ein Festbett mit einer Radikalmatrix, die sich in einem Halbach-Magneten befindet, welcher mit einer Mikrowellenkavität ausgestattet war, sodass der Polarisationstransfer ermöglicht wurde. Die so behandelte Probe fließt dann in ein mit einer Flusszelle ausgestattetes 1 Tesla NMR Spektrometer. Mit diesem ODNP-Aufbau wurden auch bei den höchsten untersuchten Durchflussgeschwindigkeiten hervorragende Ergebnisse erzielt. So konnte gezeigt werden, dass ODNP es ermöglicht, die Benchtop-NMR Spektroskopie auch zur Analyse schnell fließender Proben einzusetzen.

ODNP erfordert das Vorhandensein ungepaarter Elektronen in der Probe, dies wird meist durch Einlösen stabiler Radikale erreicht. Radikale beeinflussen jedoch die Kernrelaxation und können auch den NMR-Nachweis behindern. Dies konnte umgangen werden, indem Radikale in einem Festbett immobilisiert wurden. Die Messung von radikalfreien Proben konnte somit durch die Verwendung von ex-situ ODNP-Techniken (ODNP und NMR-Detektion erfolgen an unterschiedlichen Positionen) ermöglicht werden. Daher ist die Synthese robuster und chemisch inerter Radikalmatrizen unerlässlich. Dies

wurde durch die Immobilisierung des Radikals Glycidyloxy-Tetramethylpiperidinyloxyl (GT) mit einem Polyethylenimin (PEI)-Linker auf der Oberfläche von kontrolliert porösen Gläsern (engl. Controlled Porous Glasses: CPG) realisiert. Sowohl die Porosität der eingesetzten CPGs als auch die Größe des PEI-Linkers wurden variiert, was zu einer Reihe unterschiedlicher Radikalmatrizen für ODNP im kontinuierlichen Fluss führte. Es konnte gezeigt werden, dass CPGs mit PEI-Linkern robuste, inerte und effiziente ODNP-Radikalmatrizen liefern.

Eine weitere Methode zur Lösung des Vorpolarisationsproblems bei NMR-Anwendungen mit kontinuierlichem Fluss ist die paramagnetische Relaxationverstärkung (engl. Paramagnetic Relaxation Enhancement: PRE), welche durch die Verwendung eines T_1-Relaxationsmittels ermöglicht wird. In der vorliegenden Arbeit wurde ein PRE-Agenz eingesetzt, das wiederum durch CPGs mit PEI-Linker und GT synthestisiert wurde. Hier beschleunigte die Wechselwirkung der untersuchten Flüssigkeit mit diesem PRE-Agenz den Aufbau der Kernpolarisation vor der NMR-Detektion erheblich, sodass quantitative Messungen in kontinuierlichen Benchtop-NMR Anwendungen ermöglicht wurden. Es konnte gezeigt werden, dass das Flussregime für quantitative Messungen durch den Einsatz des synthetisierten PRE-Agenz erheblich erweitert werden konnte.

Contents

List of Symbols

Greek symbols

γ	Gyromagnetic ratio
ξ	Coupling parameter

Abbreviations

ACN	Acetonitrile
AT	Amino-tetramethylpiperidinyloxyl
BT	Benchtop
BTRM	Benchtop with radical matrix
BT+HB	Benchtop and Halbach magnet
BT+HBLoop	Benchtop and Halbach magnet with looped capillary
BT+HBODNP	Benchtop and Halbach magnet with Overhauser dynamic nuclear polarization
BT+HBRM	Benchtop and Halbach magnet with radical matrix
BDGE	Butanediol diglycidyl ether
CPG	Controlled porous glass
D	1,4-Dioxane
DNP	Dynamic nuclear polarization
EPR	Electron paramagnetic resonance
E	Signal enhancement
$E_{\mathrm{max}}^{\mathrm{static}}$	Maxmimum enhancement static
$E_{\mathrm{max}}^{\mathrm{flow}}$	Maximum enhancement in flow
f	Leakage factor
GT	Glycidyl-tetramethylpiperidinyloxyl
HT	Hydroxy-tetramethylpiperidinyloxyl
I_{Z}	Integral with enhancement
I_0	Integral
L_{Pol}	Prepolarization length
NHS	N-hydroxy-succinimide

NMR	Nuclear magnetic resonance
ODNP	Overhauser dynamic nuclear polarization
PEEK	Polyether ether ketone
PEI	Polyethylenimine
PHIP	Para-hydrogen induced polarization
PRE	Paramagnetic relaxation enhancement
r	Distance
RF	Radio frequency
RM	Radical matrix
RT	Room temperature
s	Saturation factor
S	NMR Signal with flow
S_0	NMR Signal without flow
SLIT-DNP	Solid/liquid intermolecular transfer
SNR	Signal-to-noise ratio
TEMPO	Tetramethylpiperidinyloxyl
T_1	Longitudinal relaxation time
T_1^{RM}	Longitudinal relaxation time in static contact with radical matrix
T_2	Transverse relaxation time
v	Mean flow velocity (laminar)
W	Water

1 Introduction

NMR spectroscopy offers outstanding possibilities for the investigation of technical processes, e.g. reaction and process monitoring [1–5]. A bypass approach is used often, in which a small amount of the sample is continuously pumped through a measurement loop passing through the NMR spectrometer. In these set-ups, the volume of the line between process and analysis should be small and flow-rates should be high to enable a fast transport to the analytic instrument and to obtain a high temporal resolution without disturbing the actual process. The high flexibility and compact design of benchtop NMR spectrometers make them ideally suited for such applications [6–11], as they can be installed close to the studied process. However, the analysis of a fast-flowing liquid with benchtop NMR spectrometers is particularly challenging: the small size of the permanent magnets used in benchtop NMR spectrometers leads to an incomplete polarization buildup in flowing samples due to the short residence time of the liquid in the magnetic field. This incomplete polarization buildup prevents quantitative NMR measurements and, thus, the desired accurate analysis of the composition of mixtures.

Polarization of a sample in continuous-flow can be monitored by measuring a signal S at varying flow velocity and comparing it to a signal S_0 recorded without flow. For a laminar flow, this ratio can be described by Equation 1 [12–15]:

$$\frac{S}{S_0} = 1 - \exp\left(-\frac{L_{\mathrm{Pol}}}{v \cdot T_1}\right) \tag{1}$$

where v is the average flow velocity, T_1 the longitudinal relaxation time of the nuclear-spin polarization, and L_{Pol} the polarization length of the spectrometer. For quantitative NMR measurements in continuous-flow, residence times in the magnetic field of the spectrometer of around $5{\times}T_1$ are required for complete polarization buildup, if no calibration or recalculation of polarization is applied. However, even for ^{1}H nuclei, this is on the order of many seconds for most molecules, thus heavily compromising the delay time between process and measurement. In addition to protons (^{1}H), carbon (^{13}C) or nitrogen (^{15}N) are often studied by NMR spectroscopy; these nuclei usually have significantly longer T_1 than protons and the effect of incomplete polarization buildup is even worse. In benchtop NMR spectrometers, which typically have rather short polarization lengths L_{Pol} of around 0.1 m [15], this can lead to a complete disappearance of the

signal at high flow velocities. The indirect proportionality between polarization length and flow velocity is particularly distressing for benchtop NMR spectrometers, resulting in severe restrictions on the flow rates that can be used. In general, continuous-flow NMR spectroscopy is also limited by the residence time of the flowing liquid in the active volume (i.e. the volume covered by the radiofrequency coil) of the NMR spectrometer. However, this effect is usually dominated by the prepolarization problem in continuous-flow benchtop NMR spectroscopy as even moderate flow-rates result in insufficient prepolarization. Thus, the focus here is only on the prepolarization problem.

In this thesis, the prepolarization problem was studied experimentally and counteracting methods based on ODNP and PRE were applied. A detailed examination of the combination of ODNP and benchtop NMR spectroscopy was conducted, with a new ODNP radical matrix that was synthesized based on CPGs grafted with a branched PEI-polymer and nitroxide radicals. Furthermore, a PRE agent was applied that was synthesized based on the ODNP radical matrices, with high radical loading. This PRE agent was applied for quantitative continuous-flow ^{1}H benchtop NMR spectroscopy.

2 High Flow-Rate Benchtop NMR Spectroscopy Enabled by Continuous Overhauser DNP

2.1 Introduction

To counteract the prepolarization problem in continuous-flow NMR spectroscopy, several methods have been discussed in the literature. (i) The build-up of prepolarization can be improved by using loopy flow cells which increase L_{Pol} [16, 17]. However, this leads to extended sample transfer time and therefore major delays between the process and NMR analysis, which is particularly bad for monitoring fast reactions or processes. (ii) prepolarization magnets can be used [13], which leads to similar problems as by using loopy flow cells and is technically demanding. (iii) Paramagnetic relaxation agents, e.g. stable radicals or metal complexes, can be added to the sample, such that the T_1 time of the nuclear spins is greatly decreased and the build-up of prepolarization is accelerated. There are two ways to realize this: The relaxation agent can be added to the sample [18], or the relaxation agent can be immobilized in a bed through which the sample flows [19–21]. The second way is clearly preferred: T_1 agents also affect the transverse relaxation time (T_2) and therefore cause strong line broadening of the NMR signals if present in the RF coil. An alternative to these methods is using hyperpolarization techniques.

Hyperpolarization techniques were developed and improved in the last decades to overcome the sensitivity problem of NMR spectroscopy and lead to great signal enhancement. Different techniques are available, such as para-hydrogen induced polarization (PHIP)[22–24], optical pumping [25, 26], and Dynamic Nuclear Polarization (DNP) [27–29]. In the context of NMR process monitoring, continuous hyperpolarization via Overhauser DNP is a promising and compact technique [30] that can be easily combined with benchtop NMR spectroscopy. Thereby, the flexibility of the benchtop NMR set-up is retained, as the ODNP set-up is rather small and can be mounted in the same rack as the benchtop NMR spectrometer here.

ODNP [31–33] relies on the transfer of angular momentum from highly polarized electron spins to surrounding nuclear spins. This means that unpaired electrons must be added to the sample; this can be realized in the same way as adding T_1 agents and for the same reasons as stated in the corresponding discussion above, fixed beds are preferred. Dorn et al.[34–36] were the first demonstrating ODNP in continuous flow applications with immobilized radicals. Polarization transfer between electron and nuclear spins is driven by microwave irradiation of the electron spin transitions and electron-nuclear hyperfine coupling. The microwave resonator can be placed conveniently in a Halbach magnet providing the required magnetic field [37, 38]. This set-up contains also the fixed bed with the radicals. The hyperpolarization build-up in the fixed bed happens very rapidly because it is determined by the short T_1 of the fluid in contact with the radicals. In contrast, the hyperpolarization decays only slowly in the flowing liquid after it has left the fixed bed, as then the lifetime of the hyperpolarized state is determined by the native T_1 which is much longer than the T_1 in contact with radicals. This leaves enough time for transporting the hyperpolarized liquid from the fixed bed in the Halbach magnet to the benchtop NMR spectrometer. Nevertheless, relaxation losses must be taken into account when quantitative information is to be obtained from the NMR spectra; however, corresponding methods are available [5, 39].

Versatile and chemically inert radical matrices for hyperpolarizing a wide variety of liquids are essential for the use of ODNP in process engineering applications. However, only a small number of radical matrices is available, which can be divided into two classes, depending on the carrier material that is used for the immobilization: First, silica-based radical matrices, which were used for hyperpolarization of organic solvents [36, 40, 41]. Second, hydrogel-based radical matrices, which were used for hyperpolarization of water [42–44]. For both material classes, the radical that is commonly used is 2,2,6,6-tetramethylpiperidinyloxyl (TEMPO), sometimes a linker is additionally inserted between the carrier material and TEMPO.

Here, an ODNP-enhanced benchtop NMR set-up for continuous-flow measurements was designed that enables high sensitivity NMR measurements on fast-flowing liquids in capillaries. Experiments were carried out with an equimolar acetonitrile+water mixture flowing through a capillary with an inner diameter of 0.25 mm at different volumetric flow-rates. Acetonitrile and water were chosen because of their different T_1 (especially in contact with the radical matrix) to form a demanding test case. The results obtained using ODNP were compared with those obtained with other prepolarization techniques, as well as with the base case of using only the benchtop NMR spectrometer without modifications.

2.2 Experimental Set-up and Measurements

Figure 1 shows the set-up for ODNP-enhanced continuous flow benchtop NMR spectroscopy that was designed and applied for the studies of the present work. The set-up is depicted in three panels: The left panel shows a photo of the set-up, which is mounted in a single rack that can be easily transported. The middle panel shows a scheme of the main units of the set-up: the flow first passes a fixed bed which is mounted in a Halbach magnet equipped with a microwave resonator; then it passes the benchtop NMR spectrometer, which is positioned directly below the Halbach magnet (see left panel). The right panel shows a drawing of the fixed bed containing the radical matrix.

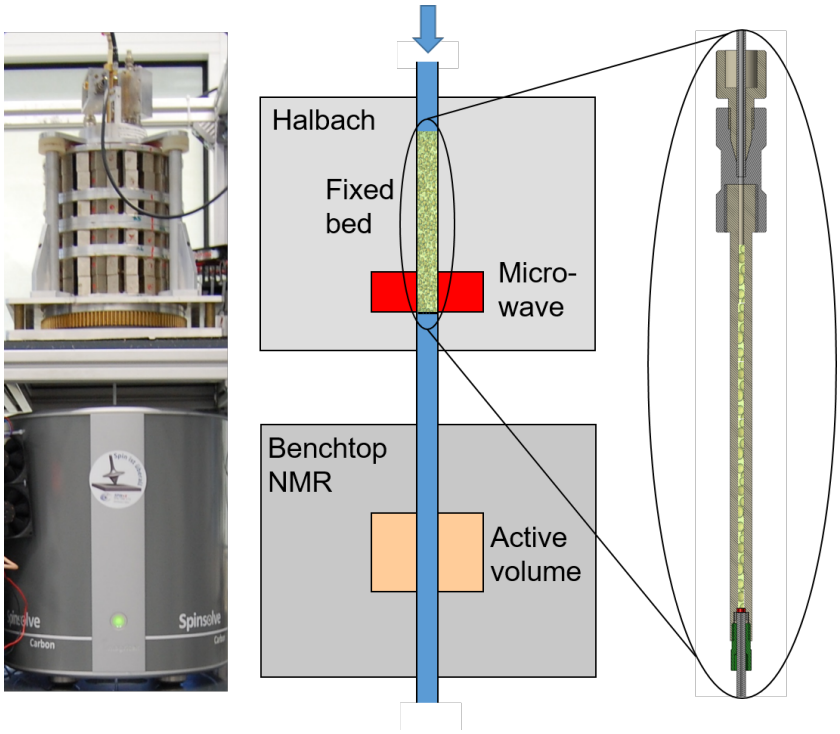

Figure 1: Left: Photo of the experimental set-up with the Halbach magnet (top) and benchtop NMR (bottom). Middle: scheme of the set-up. Flow direction is indicated by an arrow. Right: detailed drawing of fixed bed with radical matrix. The radical matrix is depicted in light green and the PEEK frit in red.

The field strength of the Halbach magnet was about 0.35 Tesla, that of the benchtop NMR spectrometer was about 1 Tesla. A Hall probe was used to measure the magnetic field strength in the equipment along the flow path. The results are presented in the Supporting Information A. The distance between the microwave cavity in the Halbach magnet and the RF coil of the benchtop NMR spectrometer is about 0.5 m.

2.2.1 Equipment

The Halbach magnet was the same as that described by Neudert et al [45]. The magnetic field strength in its center can be adjusted between 0.11 Tesla and 0.47 Tesla. The fixed bed is mounted in the center of the Halbach magnet, see Figure 1. Furthermore, an electron nuclear double resonance probehead (ENDOR) from Bruker (EN 4148X-MD4) was positioned in the Halbach magnet such that it acts on the lower end of the fixed bed, as depicted in Figure 1. The container of the fixed bed with the radical matrix is a PEEK capillary with an inner diameter of 1.00 mm. The length of the fixed bed was about 80 mm; the radical matrix was contained in the fixed bed by a PEEK frit, c.f. Figure 1, right. The length of the bed exposed to microwave radiation was about 4 mm. The microwave frequency and power were 9.67 GHz and 5 W, respectively. The electronic equipment of the set-up is described in the Supporting Information A.

The benchtop NMR instrument (proton resonance frequency of 43 MHz) was manufactured by Magritek. A PEEK capillary with 0.25 mm inner diameter was used for fluid transport from the Halbach magnet to the benchtop NMR spectrometer fulfilling the demand of small bypass volumes. NMR measurements were performed directly on the peek capillary resulting in a small sample volume of about 0.5 µL in the NMR coil. NMR experiments were performed with short acquisition times of about 400 ms in order to focus on the elucidation of the prepolarization effect and to minimize signal losses by out-flow effects of excited spins. The delay between the individual NMR scans was 3 s. The ODNP enhancement of a signal is defined as the signal with ODNP (microwave generator on) divided by that without ODNP (microwave generator off, all other parameters unchanged).

An equimolar acetonitrile+water mixture was used for the experiments. The solution was prepared gravimetrically using acetonitrile (purity ≥ 0.99 g g^{-1}) purchased from Fisher Scientific and ultrapure water (produced in our laboratory with an Elix Essential 5 purification system from Merck Millipore). The uncertainty of the composition was about 0.01 mol mol^{-1}. It was filled in a reservoir of about 500 mL and fed to the set-up described above using a HPLC pump (WADose PLUS HP) purchased from Flusys, which was equipped with a mass flow meter (Mini CORI-FLOW) that was purchased from Bronkhorst. After starting the experiment, the pump was operated until a steady state was reached. This can take up to about 2 min, as, after changing the flow-rate, the radical matrix, which is a gelly material, need time to adapt to the new conditions.

2.2.2 Set-ups for Counteracting the Prepolarization Problem

In the following, an overview of the set-ups for counteracting the prepolarization problem, is given.

Set-up BT: A reference was established by using the benchtop NMR spectrometer without any modifications for the acquisition of NMR spectra at different flow velocities. The prepolarization takes place as usual in the corresponding zone at about 1 Tesla. These experiments are labeled with BT in the following.

Set-up BTRM: A fixed bed with a radical matrix was inserted in the bore of the benchtop NMR spectrometer. It is placed directly before the RF coil, i.e. in the prepolarization zone. Hence, prepolarization takes place at 1 Tesla but with strongly decreased T_1. The Halbach magnet was not used in these experiments, which are labeled with BTRM.

Set-up BT+HB: A Halbach magnet is used together with the benchtop NMR spectrometer in order to increase the time for prepolarization. The prepolarization takes place first at 0.35 T in the Halbach magnet and then at 1 Tesla in the benchtop NMR spectrometer. These experiments are labeled with BT+HB.

Set-up BT+HBLoop: A capillary (inner diameter 1.00 mm, length 1.50 m) was looped in the large bore of the Halbach magnet. The prepolarization takes place first at 0.35 T in the Halbach magnet but with longer residence time compared to the setup BT+HB, and then at 1 Tesla in the benchtop NMR spectrometer. These experiments are labeled with BT+HBLoop in the following.

Set-up BT+HBRM: A fixed bed with a radical matrix was inserted in the Halbach magnet. Hence, prepolarization takes place first at 0.35 Tesla in the Halbach magnet but with strongly decreased T_1 and then at 1 Tesla in the benchtop NMR spectrometer. These experiments in which no microwave irradiation is applied, are labeled with BT+HBRM here.

Set-up BT+HBODNP: A fixed bed with a radical matrix was inserted in the Halbach magnet and is used as source of unpaired electrons for ODNP. The microwave is switched on and polarization transfer between electron and nuclear spins is facilitated in the Halbach magnet. These experiments are labeled with BT+HBODNP in the following.

2.2.3 Radical Matrix

The radical matrix that was used consists of the nitroxide radical TEMPO immobilized on sepharose hydrogel beads and was manufactured in our laboratory. 4-Amino-TEMPO

(purity ≥ 0.97 g g^{-1}) was purchased from Sigma-Aldrich and N-hydroxy-succinimide (NHS) activated sepharose was purchased from GE Healthcare. The procedure to immobilize the nitroxide radical onto the NHS-activated sepharose is described in the literature [42, 44, 46], but in this work it has been modified with respect to reaction time and temperature: NHS-sepharose (635 mg), which was supplied in an isopropanol suspension, was washed with HCl solution (1 mM, 10 x 5 mL) by vacuum filtration. 4-Amino-TEMPO (150 mg) was dissolved in an aqueous buffer solution (0.50 mL, 0.2 M $NaHCO_3$, 0.5 M NaCl, pH = 8.1). NHS-sepharose was added to the radical-buffer solution. The mixture was rotated slowly in a tube rotator for 90 min at 291 K. Finally, the radical matrix was washed with ultrapure water (10 x 2 mL) by vacuum filtration and was transferred to an ethanol/ultrapure water solution (30% v/v) for storage. The immobilized radical concentration in the matrix was determined to be 11.5 mM by a comparison of EPR integrals with aqueous solutions of 4-amino-TEMPO of known concentration.

To study the efficiency of the synthesized radical matrix to decrease the T_1, standard inversion recovery experiments were carried out in the benchtop NMR spectrometer with pure water, pure acetonitrile, and the equimolar mixture of these solvents in two ways: (1) without contact with the radical matrix (T_1); (2) in static contact with the radical matrix (T_1^{RM}). The results are presented in Table 1. Here, an equimolar acetonitrile+water mixture was used because of the strongly differing relaxation time of both species in static contact with the radical matrix.

Table 1: T_1 of pure water, pure acetonitrile, and of an equimolar acetonitrile+water mixture are listed, measured at 301.7 K in the benchtop NMR spectrometer. Without contact with the radical matrix (T_1) and in static contact with the radical matrix (T_1^{RM}).

Sample	T_1 / s	T_1^{RM} / s
Water	3.29	0.14
Acetonitrile	4.05	0.33
Water + (acetonitrile)	3.17	0.12
Acetonitrile + (water)	4.88	0.34

2.3 Results and Discussion

In order to determine the polarization length L_{Pol} (compare Equation 1) that is available in the benchtop NMR spectrometer used here, continuous-flow experiments were performed with water in a broad range of flow velocities. This was done with the conventional set-up BT where prepolarization takes place in the small prepolarization volume

of the benchtop spectrometer at about 1 Tesla (see Figure S1 in the Supporting Information A for the magnetic field profile in the equipment along the flow path). Three capillaries with different inner diameters (0.25 mm, 0.50 mm, 1.00 mm) were used to access a wide range of mean flow velocities. In Figure 2 the results for S/S_0 (i.e. the relative polarization, see Equation 1) at different mean flow velocities are shown. The symbols represent experimental results and were obtained as arithmetic mean of the results of 25 individual NMR acquisitions.

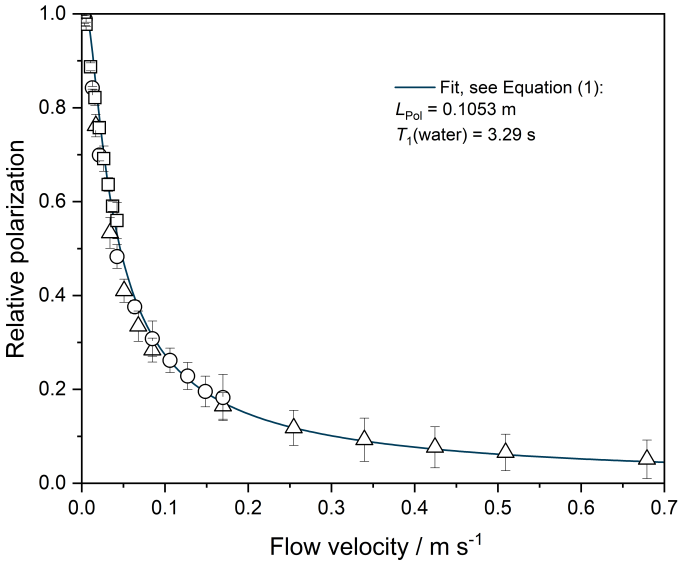

Figure 2: Relative polarization of water versus mean flow velocity is shown. The inner diameter of the capillaries are: (□) 1.00 mm, (∘) 0.50 mm, (△) 0.25 mm. The symbols are experimental results and were obtained as arithmetic mean of the results of 25 individual NMR acquisitions. The error bars indicate the standard deviation. Solid line: correlation with Equation 1.

Figure 2 clearly visualizes the severe prepolarization problem in benchtop NMR spectroscopy as already moderate flow velocities result in drastic signal losses. The relative polarization decreases exponentially with increasing flow velocity. Assuming a constant T_1 for water of 3.29 s in the benchtop NMR along the flow path, a polarization length of 0.1 m can be obtained by fitting the experimental results with Equation 1. However, this represents a rough but conservative estimation of L_{Pol} because the T_1 depends strongly on the external magnetic field, which drastically changes in the benchtop NMR spectrometer, c.f. Figure S1 in the Supporting Information A.

For the smallest capillary and the highest studied flow velocity, the benchtop NMR signal is hardly detectable which underlines the need for improved set-ups for continuous-flow benchtop NMR spectroscopy. The focus here is not on a detailed investigation of the residence time distribution inside the NMR spectrometer, but the NMR results are explained in terms of the transport time of the liquid in the set-up: From entering the benchtop NMR spectrometer to the RF coil the fluid needs around 0.6 s with a flow

velocity of around 0.34 m s^{-1}. This effective polarization time is much smaller than the T_1 of almost all liquids, therefore the built-up of equilibrium polarization is prohibited. The relative polarization of water is around 10% of the equilibrium polarization in this case and approaches the noise level at higher flow velocities. Relative errors of up to 80% were obtained in the smallest capillary at flow velocities of 0.25 m s^{-1} and more. The increasing uncertainty leads to inaccurate quantification and hampers process monitoring applications.

In order to investigate the efficiency of different prepolarization methods, further experiments with the 0.25 mm capillary were performed as this represents the most demanding test case. In ^{1}H benchtop NMR measurements without any modifications for prepolarization, the use of this tiny capillary leads to inefficient prepolarization for all studied flow velocities of 0.02 m s^{-1} and higher, c.f. Figure 2. A comparison of the experimental results that are obtained with the different set-ups (BTRM, BT+HB, BT+HBLoop, BT+HBRM, BT+HBODNP) for improving prepolarization is shown in Figure 3 and compared to the experimental results of the conventional set-up BT as a reference. Single scan ^{1}H NMR spectra are shown at a flow velocity of 0.17 m s^{-1} and 0.34 m s^{-1}. These flow velocities were chosen to show the flow-dependent effect of prepolarization because at higher flow velocities, it is not possible to acquire accurately single scan NMR spectra in the majority of the set-ups, see below.

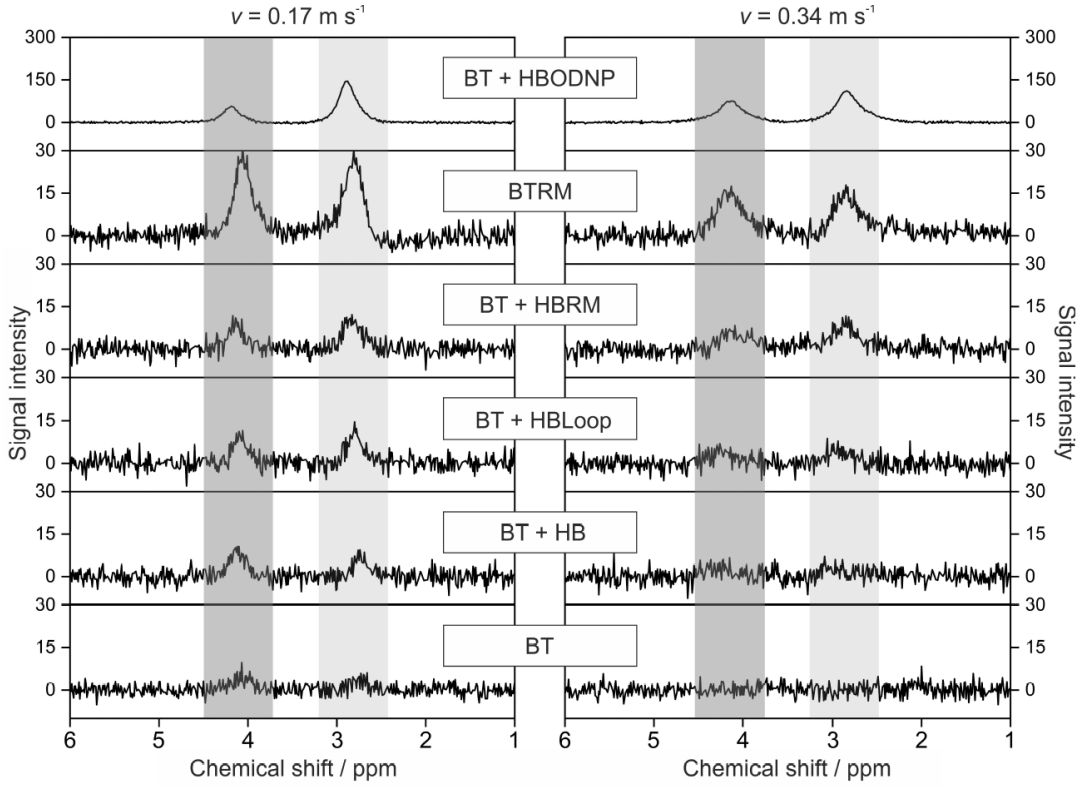

Figure 3: Comparison of single scan continuous-flow benchtop ^{1}H NMR spectra acquired in a capillary with an inner diameter of 0.25 mm at mean flow velocities (v) of 0.17 m s^{-1} and 0.34 m s^{-1}. Spectra are recorded of an equimolar acetonitrile+water mixture in different experimental set-ups, see Experimental Set-up and Measurements. The resonances of acetonitrile (light gray, around 3 ppm) and water (gray, around 4 ppm) are highlighted. The scale of the signal intensity of both ^{1}H NMR spectra that are recorded with the set-up BT+HBODNP is increased by a factor of 10.

Figure 3 shows clearly that there is a huge improvement in signal intensity for the recorded signals of acetonitrile (around 3 ppm) and water (around 4 ppm) in the benchtop NMR spectra with the set-up BT+HBODNP compared to all other set-ups. This is illustrated by the scaling and the high signal-to-noise ratio of the NMR spectra that are recorded with the set-up BT+HBODNP. The stacked ^{1}H NMR spectra in Figure 3 are discussed from bottom to top in the following. For the conventional BT measurement, the signal intensity at a flow velocity of 0.17 m s^{-1} is hardly above the noise level and at 0.34 m s^{-1} no signal at all is visible without scan accumulation. This is due to inefficient prepolarization in the small prepolarization region of the benchtop NMR magnet. For the set-up BT+HB, the additional prepolarization volume in the Halbach magnet leads to increased signal intensities. At a flow velocity of 0.17 m s^{-1} weak signals can be detected, at 0.34 m s^{-1} the signals still disappear in the noise. The prepolarization within the set-up BT+HB at a flow velocity of 0.17 m s^{-1} reached the equilibrium polarization in the Halbach magnet and no further increase of signal intensity is detected

for the set-up BT+HBLoop at this flow velocity. However, a small positive effect of the increased prepolarization time in the Halbach magnet is visible in the ^{1}H NMR spectrum at a flow velocity of 0.34 m s^{-1}. By exchanging the looped capillary in the Halbach magnet with the radical matrix, the detected signal intensity at a flow velocity of 0.34 m s^{-1} can be further increased whereas the signal intensity at 0.17 m s^{-1} flow velocity remains unaltered. This indicates that equilibrium polarization in the Halbach magnet is reached with the three set-ups (BT+HB, BT+HBLoop, and BT+HBRM). However, for the higher flow-rate prepolarization in the Halbach magnet is improved by the decreased T_1^{RM} time of the fluid in contact with the radicals that leads to a faster build-up of polarization. Using the benchtop NMR spectrometer equipped with the radical matrix in front of the RF coil (setup BTRM) leads to a further increase of detectable signal intensity. The signals of acetonitrile and water are clearly visible for both studied flow velocities. Here, the signal intensity is increased in comparison to the previously described set-ups due to the three times higher magnetic field of the benchtop NMR spectrometer compared to the Halbach magnet. The reduction of the T_1 of the fluid results in efficient prepolarization in the small prepolarization volume of the benchtop NMR spectrometer even at a flow velocity of 0.34 m s^{-1}. However, by far the highest signal intensity and signal-to-noise-ratio (SNR-ratio) is obtained with the set-up BT+HBODNP for all studied flow velocities. This is due to the fast polarization transfer of the high Zeeman polarization of the electron spins to the nuclear spins resulting in enhanced NMR signals for both components. Comparing the set-up BT with the set-ups (BTRM and BT+HBODNP) makes it clear that a strong improvement for benchtop NMR measurements in the fast flow regime can be achieved with both extended set-ups. However, ODNP leads to a boost in signal intensity and enables measurements with high SNR-ratio in the fast flow regime.

The improvement by ODNP will now be discussed separately for acetonitrile ($T_1 = 4.88$ s) and water ($T_1 = 3.17$ s) in the equimolar acetonitrile+water mixture, c.f. Table 1. Figure 4 shows the measured signal integrals for all setups over the whole studied velocity range. However, for some set-ups (BT, BT+HB, BT+HBLoop) the signals vanish into the noise level for higher flow velocities thus the data are not completely shown over the entire velocity range.

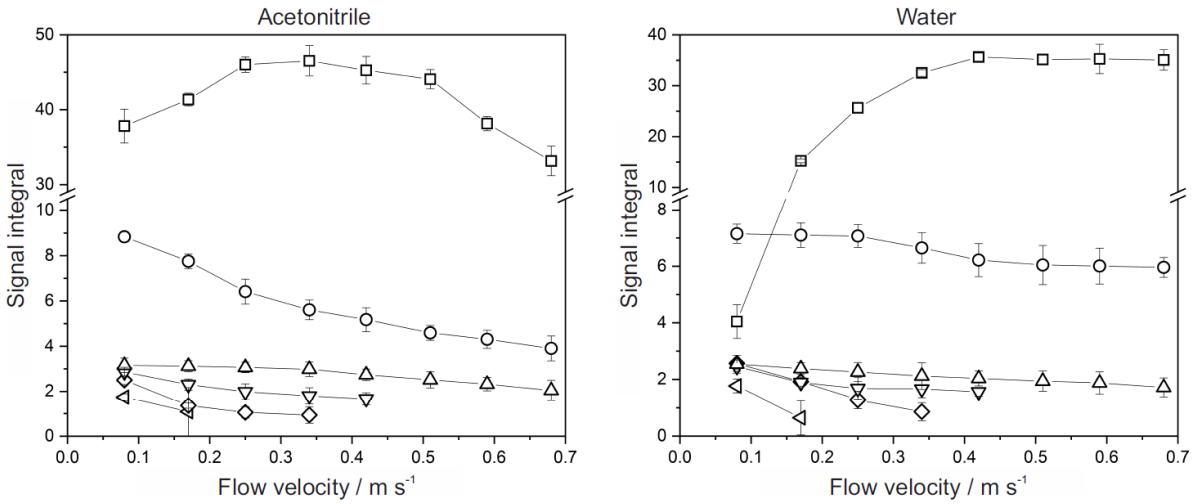

Figure 4: Flow-dependent ^{1}H NMR integrals of the acetonitrile and water signal of an equimolar acetonitrile+water mixture. Recorded with different set-ups: (□) BT+HBODNP, (○) BTRM, (△) BT+HBRM, (▽) BT+HBLoop, (◇) BT+HB, (◁) BT. Symbols are experimental results and were obtained as arithmetic mean of 10 individual NMR acquisitions. The error bars indicate the standard deviation. Solid line: guide to the eye.

For the conventional set-up BT, the integral of the acetonitrile signal decreases rapidly with increasing flow velocity due to the severe prepolarization problem. At a flow velocity of 0.25 m s^{-1} the detection of a distinct signal is not possible with single scan acquisition because the residence time in the prepolarization volume of the benchtop NMR magnet is too short. Using the Halbach magnet for additional prepolarization with the set-up BT+HB enables to measure up to a flow velocity of 0.34 m s^{-1}, but still the residence time in the prepolarization volume of the Halbach and benchtop NMR magnet is too short for a significant build-up of polarization. If the residence time in the Halbach magnet is increased by using a looped capillary, single scan NMR acquisition up to a flow velocity of 0.42 m s^{-1} is possible. Only by using the radical matrix with the set-ups (BT+HBRM, BTRM, BT+HBODNP) enables NMR measurements over the entire range of flow velocities studied here. With the set-up BT+HBRM, integrals of the acetonitrile signal are constant up to a flow velocity of 0.34 m s^{-1}. Here, the build-up of prepolarization in the Halbach magnet is efficient to reach equilibrium polarization. Relaxation of prepolarization during the transport of acetonitrile to the benchtop NMR spectrometer is counterbalanced by an additional build-up of polarization in the small prepolarization volume of the benchtop NMR magnet. At higher flow velocities the integral of the acetonitrile signal decreases again due to the decreasing residence time in the magnetic field of the Halbach magnet. As already mentioned before, the integral of the acetonitrile signal measured with the set-up BTRM is increased in comparison to the previously described set-ups due to the prepolarization in the higher magnetic field of the benchtop NMR magnet. However, in contrast to the set-up BT+HBRM the

set-up BTRM does not result in constant signal integrals for a range of flow velocities because of the small prepolarization volume of the benchtop NMR magnet, indicating that the equilibrium polarization is not reached even for small flow velocities in this set-up. Finally, the measurement series with the set-up BT+HBODNP will be discussed. For small flow velocities, an increase of the measured integral is observed because of decreasing relaxation of hyperpolarized acetonitrile during the transport from the ODNP site to the benchtop NMR spectrometer. At flow velocities between about 0.25 m s^{-1} to 0.42 m s^{-1} a plateau of integrals is observed, which represents a trade-off between relaxation during the transport and build-up of hyperpolarization. For higher flow velocities a decrease of the signal integral is observed, which is caused by an incomplete hyperpolarization build-up via ODNP. The build-up of hyperpolarization depends on the T_1^{RM} time, see Table 3, and is therefore only limited for very high flow velocities. Here, the residence time in the microwave resonator, which is only 4 mm long, is not sufficient to reach a full hyperpolarization build-up. However, for the entire range of flow velocities studied here, the signal integrals accomplished by this set-up are at least increased by a factor of four compared to the best measurement without ODNP. Compared to the conventional set-up BT the signals recorded with the set-up BT+HBODNP are at least increased by a factor of around 20. Moreover, ODNP enables to measure in the fast flow regime with very good SNR-ratios, in which measurements with the conventional set-up BT are not feasible at all.

Figure 4 shows similar trends for the flow-dependent signal integrals of water for the different set-ups, as already discussed for acetonitrile. The differences are mainly related to the shorter T_1 of water, see Table 1. For the set-ups (BT, BT+HB, BT+HBLoop, BT+HBRM) hardly any differences can be worked out for the acetonitrile and water measurements, except for a slightly minor prepolarization problem. This effect can be mainly seen in the detected integrals of the water signal with the set-up BTRM. Up to a flow velocity of 0.25 m s^{-1}, a constant value of the detected integrals of the water signal is observed because equilibrium polarization in the benchtop NMR magnet is reached. As expected, a strong increase of the measured signal integrals of water is observed using hyperpolarization via ODNP, compared to all previously discussed set-ups that rely on thermal polarization of protons. ODNP is especially well suited for high flow velocities where NMR measurements with conventional benchtop NMR spectroscopy are not possible anymore.

Figure 5 shows continuous-flow ODNP-enhanced benchtop ^{1}H NMR spectra of an equimolar acetonitrile+water mixture over the entire range of flow velocities studied here. It can be observed that the flow-induced-broadening of NMR signals with increasing flow velocity leads to an overall decrease in signal intensity. This underlines once more the benefit of hyperpolarization for continuous-flow benchtop NMR spectroscopy, as NMR

spectra with high SNR-ratios are particularly hard to detect for broad NMR lines.

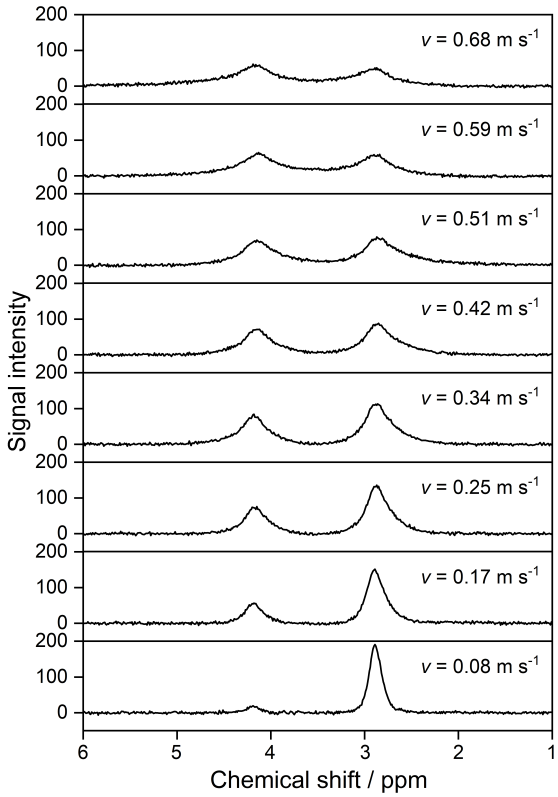

Figure 5: ^{1}H NMR spectra of continuous-flow ODNP-enhanced measurements in a capillary with an inner diameter of 0.25 mm. Spectra are recorded of an equimolar acetonitrile+water mixture at mean flow velocities of 0.08 m s^{-1} up to 0.68 m s^{-1} with the setup BT+HBODNP. The resonances of acetonitrile (light gray, around 3 ppm) and water (gray, around 4 ppm) are highlighted.

The signal intensity of acetonitrile decreases with increasing flow velocity, whereas the integrals increase slightly up to a flow velocity of 0.34 m s^{-1}. At higher flow velocities, an inefficient build-up of hyperpolarization of acetonitrile can be observed because of the relatively long T_1^{RM} time even in contact with the radical matrix. Contrary to acetonitrile, the signal intensity of water increases with flow velocity, as well as the integral of the signal. Here, the dominant effect is the relaxation of hyperpolarized water during the transport from the ODNP site to the benchtop NMR spectrometer. This effect is more relevant for water in comparison to acetonitrile due its shorter T_1, c.f. Table 1 and Figure 4. At the highest flow velocity of 0.68 m s^{-1} a strong broadening of NMR signals can be seen, but still both components can be easily detected with single scan acquisition. The best ODNP enhancement for both components is achieved at flow velocities of 0.34 m s^{-1} to 0.42 m s^{-1}, whereas with conventional benchtop NMR spectroscopy no signals at all are detectable at this range of high flow velocities with single scan acquisition.

Finally, the reproducibility of continuous-flow ODNP-enhanced NMR measurements is

demonstrated. Figure 6 shows ^{1}H NMR integrals of water at a flow velocity of 0.17 m s^{-1}.

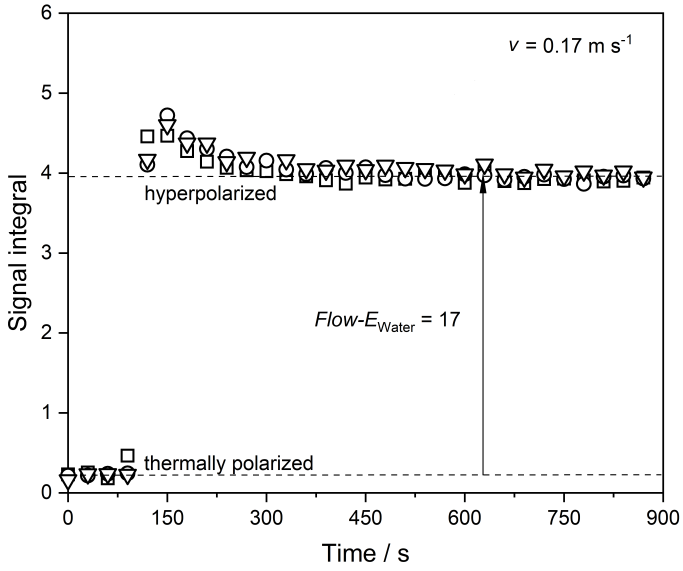

Figure 6: ^{1}H NMR integrals of water at a mean flow velocity of 0.17 m s^{-1} recorded with the setup BT+HBODNP. The symbols are the experimental results of three individual fixed beds that contain the radical matrix, see Figure 1. The first data points are measured without microwave irradiation (thermally polarized), after 90 s the microwave is switched on (hyperpolarized).

The symbols are experimental results of three individual fixed beds that contain the radical matrix. The first data points are measured without microwave irradiation (thermally polarized) and after 90 s the microwave is switched on (hyperpolarized). After 150 s the ODNP-enhanced integrals of the water signal are on a plateau. The reproducibility on this plateau is very high over a period of time of more than 10 min. The ODNP-enhanced integrals of the water signal decreases slightly after hyperpolarization is started. This is a consequence of a slight frequency drift of the microwave resonator because of heating, whereby the saturation of the electron spin transition is not perfectly matched anymore. After 150 s the cooling of the ODNP resonator with dehumidified nitrogen stabilizes the microwave frequency drift and the ODNP-enhanced integrals of the water signal remain constant. The reproducibility is very high over a period of time of more than 10 min. The enhancement of continuous-flow benchtop NMR with ODNP (microwave on) at a flow velocity of 0.17 m s^{-1} is around 17 calculated relative to the conventional benchtop NMR acquisition (microwave off).

2.4 Conclusions

An overview of different approaches to counteract the prepolarization problem in continuous-flow benchtop NMR spectroscopy has been presented, i.e. the use of a prepolariza-

tion magnet, a loopy flow cell, incorporation of a fixed bed with an immobilized T_1 agent, and hyperpolarization via ODNP. The experimental results were compared to conventional benchtop NMR spectroscopy, where the signal already vanishes for moderate flow velocities because of the small prepolarization volume of the compact instrument.

The use of a prepolarization magnet and a loopy flow cell already extended the accessible range of flow velocities compared to using the benchtop NMR spectrometer without modifications. However, the obtained SNR-ratios are still very small and the range of accessible flow velocities is limited. By incorporating a T_1 agent (here an organic matrix with covalently bound radicals) in the flow path before the liquid enters the RF coil of the benchtop NMR spectrometer, the polarization build-up happens very rapidly and directly at the field strength of the benchtop NMR magnet. This enables NMR measurements with high SNR-ratios over the entire range of flow velocities studied in this work. The method is promising for process monitoring applications as it allows for a direct quantitative analysis of the obtained NMR spectra in order to elucidate the composition of reaction mixtures. Moreover, it is cheap and can be easily implemented into a common benchtop NMR spectrometer.

However, a large improvement of the detected signal intensities especially in the fast flow regime, was realized by the combination of ODNP with continuous-flow benchtop NMR spectroscopy. The reproducibility of the presented method is high and allows stable measurements over a long period of time. The improvement on the accessible range of flow velocities of continuous-flow benchtop NMR spectroscopy is especially important for measurements of very fast reactions or processes, where the residence time and volume in the bypass line has to be as small as possible. The sample volume in this set-up is on the µL-scale, but still NMR spectra with very good SNR-ratios are recorded in single scan acquisition. The quantification of the ODNP-enhanced measurements was not in the scope of this work. For this, two effects must be particularly considered: The T_1 relaxation of the hyperpolarized molecules during the transport from the ODNP to the detection site and molecule-specific enhancements because of different hyperfine interactions with the radical matrix. For quantification of the first effect, some methods are available in the literature that can be adopted [5, 39]. In a first approach, the second effect can be taken into account by means of calibration.

The ODNP method enables further applications, as e.g. continuous-flow NMR spectroscopy of nuclei with high T_1 or insensitive nuclei, like ^{13}C, which is not feasible by conventional benchtop NMR spectroscopy. Thus, ODNP is envisaged to enable new applications of continuous-flow benchtop NMR spectroscopy.

3 Functionalized Controlled Porous Glasses for Producing Radical-Free Hyperpolarized Liquids by Overhauser DNP

3.1 Introduction

Currently, Overhauser DNP (ODNP) is increasingly used in combination with compact NMR instruments [15, 30, 47–49], because ODNP units are rather small and add only moderately to the weight and size of the overall NMR system. Compact NMR systems are mainly based on permanent magnets and allow a very flexible use of NMR spectroscopy because a dedicated laboratory infrastructure and cryogenic coolants are not needed. Many applications can profit from compact NMR spectrometers, which provide fast on-spot sample characterization, from standard laboratory analysis to online process monitoring. The use of permanent magnets, however, limits the maximal achievable magnetic field strength and, therefore, the signal-to-noise ratio (SNR) that in turn restricts applications. The situation becomes even worse when flowing samples have to be investigated, as it is often the case in reaction and process monitoring applications. [2, 16, 39, 50–55].

The typical ODNP experiment under continuous-flow is carried out as follows: The flowing sample passes first the ODNP unit containing a fixed bed of immobilized radicals for hyperpolarization build-up before it enters the NMR spectrometer. Immobilization of radicals is necessary in these set-ups because the presence of free radicals reduces the nuclear T_1 of the liquid and thereby also the lifetime of the accomplished hyperpolarization during the transport time from the ODNP unit to the NMR detector. Consequently, a major part of the enhanced signal would be lost due to rapid T_1 relaxation during the transport time if dissolved radicals were used. Moreover, radicals affect also the transverse relaxation time T_2 resulting in line broadening of the NMR signals if present during NMR detection. Dorn et al. [34–36] were the first to present and optimize ODNP on con-

tinuously flowing samples. They introduced the abbreviation SLIT-DNP (Solid/Liquid Intermolecular Transfer) because they used radicals immobilized on silica-based solids as ODNP polarizations agents. Silica radical matrices [34, 36, 40, 56] were studied by using various linker structures for coupling TEMPO radicals on the surface of the solids. Linkers that provide a large distance between the radicals and the solid surface worked best in these studies. More recently, other groups have employed continuous-flow ODNP for clinical purposes, i.e. for the generation of a continuous stream of hyperpolarized water as MRI contrast agent, by using hydrogel-based polarization matrices [43, 46, 57–59]. In these approaches, mainly sepharose was used as hydrogel matrix for TEMPO radicals. The Han group further optimized sepharose-TEMPO matrices by introducing an additional polyelectrolyte linker, which led to a strong increase in the ODNP signal enhancement [43, 60].

Although the use of immobilized radical matrices is essential for continuous-flow ODNP, only a very small number of radical matrices has been described in the literature so far. The systems can roughly be divided into two groups, depending on the used matrix: (1) based on silica and (2) based on hydrogels, with sepharose as the most prominent example. For applying continuous-flow ODNP for process monitoring studies, radical matrices should fulfill the following requirements: sufficient radical loading, high mobility of radicals, easy access of the target molecules to the radicals, chemical stability, compatibility with a wide range of solvents, temperature stability, pH stability, long-term stability, and a morphology that enables using them in fixed beds with favorable flow characteristics. Thus, hydrogels like sepharose have several drawbacks, e.g. poor chemical stability, strong temperature, pH, and pressure dependence, and limited applicability in non-aqueous solutions. In water-free systems the radical-target molecule contact is substantially diminished due to poor swelling of the hydrogel, resulting in bad ODNP efficiency. Silica-based radical matrices, on the other hand, fulfill most of the above-mentioned requirements. However, if porous solids such as silicas are used for radical immobilization, special care has to be taken that materials are chosen for which the influence of the pore walls on the T_1 relaxation time of the liquid is small. McCarney et al. [46] have shown that the ODNP efficiency of commercially available spin labeled silica matrices (with extremely high radical loadings of up to 900 mM) is poor because extra modes of proton relaxation in porous materials already decrease the native T_1 time by around 90%; even without immobilized radicals. These matrices had very small pore sizes of 6 nm and 10 nm, thus T_1 relaxation via the pore walls was extremely efficient and the electron-driven part of the nuclear T_1 was not dominant. To avoid this effect, porous matrices with larger pore sizes have to be chosen for ODNP applications. Unfortunately, this reduces the specific surface area of the porous materials and, thus, the number of possible binding sites for immobilization, so that it is hard to

achieve sufficiently high radical loadings, which are required for a high ODNP efficiency.

Therefore, new silica-based radical matrices with polyethyleneimine (PEI) linkers and immobilized the nitroxide radical 4-glycidyloxy-2,2,6,6- tetramethyl-piperidine-1-oxyl (GT) were synthesized for continuous-flow ODNP applications and tested. The aim was to create materials suitable for process monitoring applications. Ccontrolled pore glasses (CPGs) were used as matrix, with large pore sizes of 50, 100, and 200 nm, because they fulfill the above-mentioned design criteria: they are chemically inert, stable in a wide temperature and pH range, have a narrow pore size distribution, provide fairly weak wall relaxation and good flow characteristics. However, the number of binding sites on these CPGs for the attachment of radicals is not sufficient for obtaining a good ODNP. Therefore, a synthesis strategy was developed in which first PEI was attached to the binding sites of the CPGs. The polymer PEI in turn provides many binding sites for the covalent attachment of radicals. PEI is also known for high-performance immobilization of bio-catalysts [61–64]. In the last step, the nitroxide radical GT was immobilized on the PEI-grafted CPGs. Both the porosity of the CPGs and the size of the PEI-linker were varied in subsequent syntheses. Furthermore, the radical-target molecule contact can be varied in these systems by adjusting the pH, because in the protonated form, at low pH, the PEI-linker is stretched. The stretched form leads to improved spatial expansion of the PEI-linker and, therefore, to an easier accessibility of the immobilized radicals. This approach combines the ideas of Dorn et al. [40] (large radical-surface distance) and Han et al. [43] (using a polyelectrolyte linker) for optimal ODNP efficiency and adds on top of this the possibility to easily achieve high radical loadings in the systems.

First, a short introduction in the basic Overhauser DNP theory is given, as this is mandatory to understand the influence of the different factors impacting ODNP efficiency. Thereafter, the synthesis of CPG radical matrices is described and the ODNP set-up used for the studies is explained. In the results and discussion section, the results of the experimental studies on the influences of different factors that determine the ODNP efficiency are presented and compared to literature values, where possible. This comprises: the influence of the radical loading, which was studied by EPR spectroscopy, and the ODNP leakage factor, which was determined by T_1 inversion recovery measurements. ODNP experiments in static contact with the radical matrix and in continuous-flow are presented in which the microwave power was varied, as well as results from experiments in which the pH was varied to study the influence of the conformation of the PEI-linker.

3.2 Overhauser Dynamic Nuclear Polarization

ODNP relies on the transfer of polarization of electron spins to surrounding nuclear spins and was already assumed by Albert Overhauser in 1952 [65–67]. The polarization transfer is driven by microwave irradiation of electrons and electron-nuclear hyperfine coupling, which is of dipolar nature for protons and nitroxide radicals. The detailed theory of ODNP is given elsewhere [31, 33] only essential relations are introduced below. The ODNP enhancement (E) of the NMR signal is the ratio of signals of hyperpolarized measurements I_Z (microwave on) and those of thermally polarized measurements I_0 (microwave off) and is calculated as given by Equation 2:

$$E = \frac{I_Z}{I_0} = 1 - \xi s f \frac{|\gamma_S|}{\gamma_I}, \tag{2}$$

where s is the saturation factor, ξ the coupling factor, and f the leakage factor. The constant γ_I denotes the gyromagnetic ratio of the nucleus and γ_S that of the electron. The maximal theoretical enhancement for ^{1}H ODNP is about 660 (i.e. the ratio of γ_I and γ_S), but the other parameters are the limiting factors. The coupling factor ξ, which is a measure of the hyperfine interaction between the electron and nuclear spin, ranges between -1.0 for pure scalar coupling and 0.5 for pure dipolar coupling. For the nitroxide-based radical matrix that was used in the present work with ^{1}H ODNP the dipolar interaction is dominant [31], thus the maximum achievable enhancement is limited to about -330 [68]. The coupling factor ξ depends on the temperature and magnetic field strength [31, 33, 69] and can be determined with several methods: (1) molecular dynamic simulations can be performed, which, however, require modelling assumptions and are computationally expensive [70–72], especially in SLIT-DNP; (2) T_1 relaxation dispersion data can be used [73–76]; (3) recalculation from measured ODNP enhancements can be done, if the other ODNP parameters are known. The latter approach provides only a rough estimation because of temperature effects occurring during microwave irradiation. The saturation factor s describes the efficiency of the saturation of the electron spins and strongly depends on the applied microwave power. It ranges between 0 and 1. It can be determined with several methods: (1) pulsed ELDOR measurements can be performed for precise determination [77–79] (2) Prisner et al. used the influence of the paramagnetic shift by applied microwave power to calculate the saturation factor [74, 80, 81] (3) Recalculation with ODNP data, if other ODNP parameters are known. The leakage factor f denotes the effectiveness of electron-driven nuclear spin relaxation and ranges also between 0 and 1. This ODNP parameter is directly accessible via NMR and is calculated from:

$$f = 1 - \frac{T_1^{\mathrm{RM}}}{T_1}, \tag{3}$$

where T_1^{RM} denotes the longitudinal relaxation time of the nuclear spin in static contact with the radical matrix and T_1 the longitudinal relaxation time in static contact with the PEI-grafted CPG matrix, but without immobilized radicals. Reaching a value of $f = 1$ indicates the desired dominant relaxation via the electron spins. This is achieved at sufficiently high radical concentrations, e.g. for the widely used 4-hydroxy-TEMPO radical for concentrations of around 20 to 30 mM.

3.3 Materials and Methods

3.3.1 Radical Matrix Design

The radical matrices designed in the present work consist of the nitroxide radical glycidyloxy-tetramethylpiperidinyloxyl (GT) immobilized on aminopropyl-functionalized CPGs and were synthesized in our laboratory. In addition, to immobilize GT directly on aminopropyl-functionalized CPGs, the PEI-linker and the intermediate linker 1,4-butanediol diglycidyl ether (BDGE) were used as coupling agents. Figure 7 shows a simplified immobilization scheme that is divided into three steps, i.e. step I: coupling of BDGE-linker on aminopropyl-functionalized CPGs, step II: coupling of PEI on BDGE-grafted CPGs, step III: immobilization of GT. The detailed synthesis is described in the Supporting Information B. In the first case, of immobilizing GT directly on the CPG surface, the first two steps in Figure 7 were omitted and the nitroxide radical was immobilized in step III on aminopropyl-functionalized CPGs. For the second case, of immobilizing GT indirectly with PEI-linker and BDGE-linker, the intermediate linker BDGE was covalently bound to provide glycidyl-functionalized CPGs in step I, and afterwards PEI was added in step II. All reactions were solely carried out at room temperature (RT) in methanol.

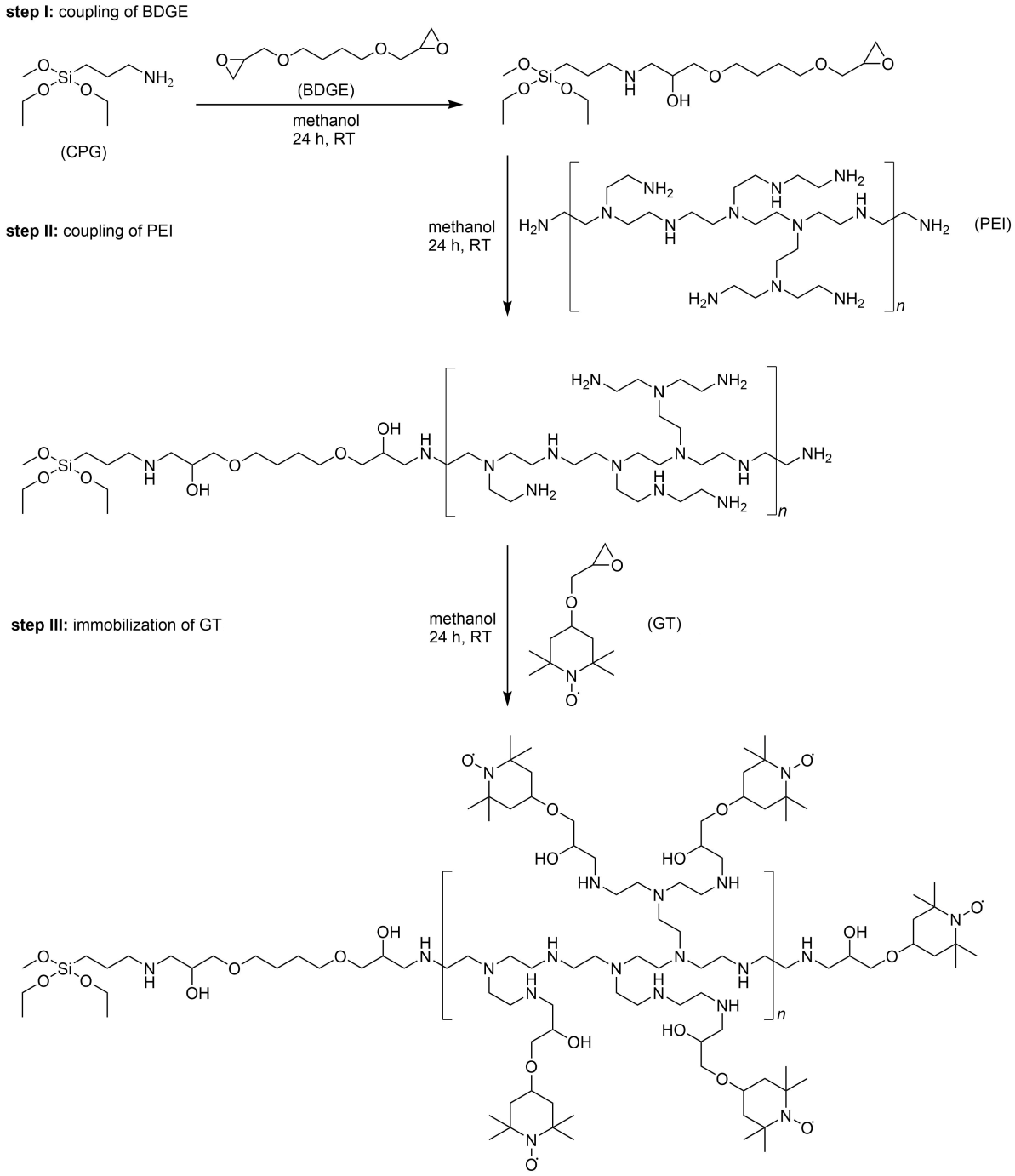

Figure 7: Scheme of the three-step immobilization procedure: (1) coupling of BDGE on aminopropyl-functionalized CPGs; (2) coupling of PEI on glycidyl-functionalized CPGs; (3) immobilization of GT. In this work, radical matrices with immobilization of GT directly on the surface of aminopropyl-functionalized CPGs (only step III) and with immobilization indirectly on CPGs with BDGE-linker and PEI-linker were synthesized (step I to step III). All reactions were solely performed at room temperature (RT) in methanol.

Aminopropyl-functionalized CPGs with three different pore sizes (50, 100, and 200 nm) were used as starting materials with surface areas according to the manufacturer's data of 25 $m^2\ g^{-1}$, 51 $m^2\ g^{-1}$, and 69 $m^2\ g^{-1}$. PEI-linker with different molecular masses,

800 g mol^{-1} (PEI800) and 25000 g mol^{-1} (PEI25000), were attached to the CPGs. The coupling reactions in the presented immobilization procedure of GT take place exclusively with the reaction of epoxy- and amino-groups in all steps. A distinction in the matrix design is achieved with the following ways of radical immobilization: (i) directly on the surface of the CPGs; (ii) indirectly with short PEI-linker (PEI800); (iii) indirectly with long PEI-linker (PEI25000). In this way, nine different radical matrices were synthesized. The procedure to quantify the amount of immobilized GT by EPR spectroscopy is provided in the Supporting Information B .

3.3.2 ODNP Set-up

The ODNP-enhanced continuous-flow NMR set-up is shown in a simplified overview in Figure 8. The liquid passes first a fixed bed with the radical matrix that is placed in a 0.35 Tesla Halbach magnet [15] which is equipped with an ENDOR probehead. Here, microwave irradiation and, thus, ODNP polarization build-up is accomplished. The liquid flows then through a PEEK capillary (250 µm inner diameter) to a 1 Tesla benchtop NMR spectrometer, in which the capillary simply passes the bore and is used as flow probe.

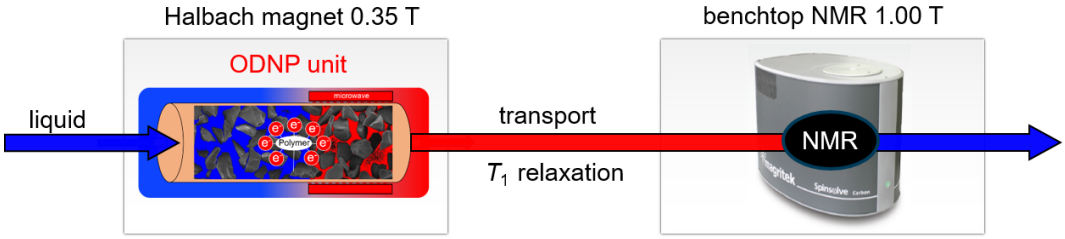

Figure 8: Scheme of the set-up for continuous-flow benchtop NMR measurements with ODNP unit. ODNP is performed at 0.35 Tesla in a Halbach magnet. ODNP measurements are performed in two ways: (1) static ODNP with hyperpolarization directly in the Halbach magnet that is equipped with an ENDOR probehead for simultaneous microwave irradiation and NMR detection and (2) continuous-flow ODNP, where hyperpolarization is accomplished in the Halbach magnet and NMR detection in the 1 Tesla benchtop NMR spectrometer (transport distance is around 0.5 m). A HPLC pump is used to set up the liquid flow.

Besides continuous-flow experiments [15], also static experiments were carried out [45]. Static ODNP measurements were performed using the ENDOR probehead in the Halbach magnet also as NMR detector, i.e. without using the benchtop NMR spectrometer. Experimental procedures are described in the Supporting Information B.

3.4 Results and Discussion

3.4.1 Radical Matrix Characterization

Table 2 provides an overview of radical matrices synthesized in this work, CPG-GT (without PEI), CPG-PEI800-GT, and CPG-PEI25000-GT that were used in ODNP-enhanced NMR spectroscopy. Radical loadings of all radical matrices are provided which were measured by EPR spectroscopy and are listed in Table 2.

Table 2: Concentrations c of immobilized GT on CPGs with pore size d of 50, 100 and 200 nm from EPR measurements. Radical matrices were synthesized without linker (CPG-GT), with PEI800-linker (CPG-PEI800-GT), and with PEI25000-linker (CPG-PEI25000-GT).

Radical matrix	CPG-GT	CPG-PEI800-GT	CPG-PEI25000-GT
d / nm		c / mM	
50	1.0	7.5	37.4
100	0.3	3.5	31.9
200	0.2	2.3	12.4

The radical loadings were calculated by comparison of EPR integrals with aqueous solutions of GT of known concentrations (see Supporting Information, where also representative EPR spectra are provided). The radical loading for each set of CPGs increases with decreasing pore size. This trend is expected as also the surface area and, thus, the binding capacity of the CPG based materials increases with decreasing pore size. Furthermore, a significant increase of the immobilized radical loading is achieved by using PEI. The desired radical loading (of about 30 mM) for ODNP was achieved with radical matrices of the type CPG-PEI25000-GT with a pore size of 100 and 50 nm.

Table 3 lists T_1 values of acetonitrile and water in static contact with the radical matrices and with the CPG matrix without immobilized radicals, CPG, CPG-PEI800, and CPG-PEI25000 that were used to study the relaxation behavior dependent on pore size of CPGs and size of the PEI-linker.

Table 3: Longitudinal relaxation times T_1 of water (W) and acetonitrile (ACN) in static contact with CPGs with pore size d of 50, 100 and 200 nm at 1 Tesla and 301.7 K. T_1^{RM} indicates values obtained in contact with the radical matrix, T_1 indicates values in contact with PEI-grafted CPG matrices without radicals.

Radical matrix	CPG-GT		CPG-PEI800-GT		CPG-PEI25000-GT	
d / nm	T_1^{RM}(W) /s	T_1^{RM}(ACN) /s	T_1^{RM}(W) /s	T_1^{RM}(ACN) /s	T_1^{RM}(W) /s	T_1^{RM}(ACN) /s
50	0.95	1.85	0.19	0.54	0.08	0.09
100	1.48	2.47	0.34	0.72	0.09	0.14
200	1.99	3.01	0.48	0.97	0.16	0.25
Matrix	CPG		CPG-PEI800		CPG-PEI25000	
d / nm	T_1(W) /s	T_1(ACN) /s	T_1(W) /s	T_1(ACN) /s	T_1(W) /s	T_1(ACN) /s
50	1.73	2.78	1.71	2.55	1.27	1.89
100	1.97	2.86	1.77	2.72	1.49	2.33
200	2.08	3.10	1.90	2.94	1.51	2.51

The next step is to investigate the efficiency of CPGs for decreasing T_1 and to finally calculate ODNP leakage factors. Therefore, standard inversion recovery measurements were carried out in a 1 Tesla benchtop NMR spectrometer with pure water and pure acetonitrile in two ways: (1) in static contact with the radical matrix (T_1^{RM}); (2) in static contact with the CPG matrix, without immobilized radicals (T_1). Acetonitrile and water were chosen as target molecules because of their different T_1 values. As stated before, it is mandatory for high ODNP efficiency that the T_1 of nuclear spins is dominated by the interaction with electron spins, i.e. T_1^{RM} have to be much smaller than T_1. This condition is best fulfilled if the influence of wall relaxation and relaxation via the polymer PEI is small for target molecules. Table 3 shows that the T_1 values of bulk water (native T_1 = 3.0 s) is decreased by 42% by the CPG matrix with the smallest pore diameter of 50 nm without radicals and by around 31% for the CPG matrix with the largest pore diameter of 200 nm without radicals. Thus, also in the present study, an increasing effect of wall relaxation with decreasing pore size was found, as it becomes also obvious from the data of bulk aceto-

nitrile (native T_1 = 4.0 s).

Moreover, Table 3 shows that also the coupling of BDGE and PEI to the surface of the CPGs results in a slight decrease of the T_1 values of water and acetonitrile. This effect becomes stronger with increasing size of the PEI-linker, but is still moderate compared to the influence of the pore walls. Thus, the T_1 reduction in our systems is much less pronounced than in the silica-based systems with very small pore sizes described in the literature [46] (pore size of 6 and 10 nm, T_1 drop by wall relaxation of 90%). T_1 in our systems remain long enough to allow for sufficient electron-driven relaxation. It is clearly shown that with increasing radical loading a very substantial decrease of the relaxation times of water and acetonitrile is achieved, cf. Table 2 and Table 3, as it is necessary for high ODNP efficiency; the best results were achieved with the radical matrix CPG-PEI25000-GT with the smallest pore size of 50 nm and the highest amount of immobilized GT.

The positive trend in the T_1 data manifests itself in the calculation of the leakage factors, cf. Equation 3. Leakage factors are close to 1 if nuclear T_1 is dominated by unpaired electrons which is achieved at sufficient high radical loadings (20-30 mM, c.f. Supporting Information B for dissolved TEMPO radicals in water and acetonitrile). For our CPGs, high radical loadings and optimal leakage factors were achieved only for CPG-PEI25000-GT with radical loadings ranging from 12 to 37 mM. For this reason, in subsequent experiments only materials of the type CPG-PEI25000-GT were tested. The leakage factors for these systems are listed in Table 4 and show promising values of up to 0.94 for both solvents. This means that our strategy of choosing fairly large pore sizes of the CPGs and providing additional radical binding sites via introduction of the PEI-linkers has worked well. The leakage factors of all other synthesized materials in acetonitrile and water are shown in the Supporting Information B.

Table 4: ODNP parameters of synthesized CPG radical matrices of the type CPG-PEI25000-GT. E_{max}^{static} values are calculated from static ODNP measurements that are dependent on microwave power with extrapolation to infinite microwave power. Coupling factors were estimated with the assumption of saturation factors equal to 1 and are also listed.

Pore size / nm	f	E_{max}^{static}	ξ
		Water	
50	0.94	-77.6	0.13
100	0.94	-68.3	0.11
200	0.92	-62.6	0.10
		Acetonitrile	
50	0.95	-41.1	0.07
100	0.94	-27.4	0.05
200	0.90	-13.2	0.02

3.4.2 Static ODNP

The performance of the synthesized radical matrices in ODNP were studied with static ODNP-enhanced NMR measurements with varying microwave power using radical matrices of the type CPG-PEI25000-GT directly in the ENDOR probehead in microcapillaries. The results are shown in Figure 9. Low microwave power levels in the range of around 0.5 to 2.5 W were used because otherwise significant sample heating would be introduced, which results in increasing coupling factors [69], and often leads to misinterpreted results.

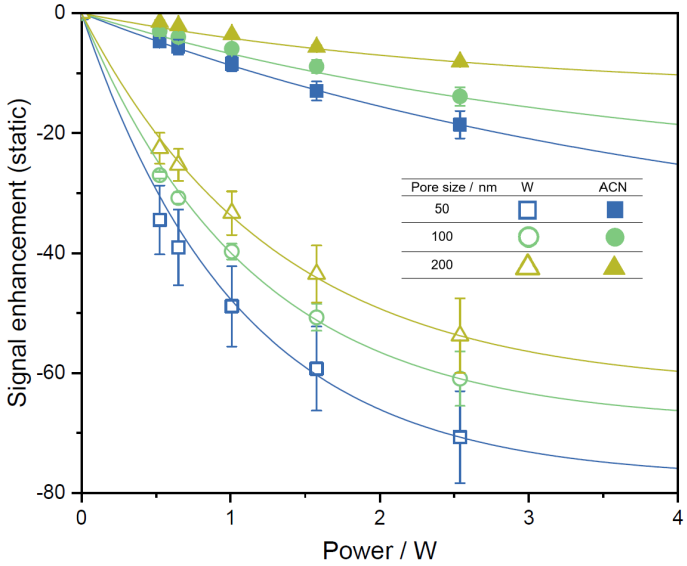

Figure 9: Results from static ODNP measurements with water (W) and acetonitrile (ACN) obtained with CPG-PEI25000-GT of different pore sizes and different applied microwave power values. The symbols are experimental results and were obtained as the arithmetic mean of the measurements of five individual samples. The error bars indicate the standard deviation. Solid lines: extrapolation to infinite microwave power [31, 82].

Figure 9 shows that high absolute ODNP enhancements were achieved with studied CPGs, especially with those with the lowest pore size (50 nm), for which the highest measured absolute values were about -20 for acetonitrile (ACN) and -70 for water (W). The large differences in the enhancement values measured for water and acetonitrile is explained by the different hyperfine interaction of the methyl group of acetonitrile and the water protons with the TEMPO radical, which is in line with the findings for T_1^{RM}, cf. Table 3. TEMPO radicals are particularly well suited for the hyperpolarization of water. From ODNP data with increasing microwave power, $E_{\mathrm{max}}^{\mathrm{static}}$ values for the enhancement at infinite microwave power were extracted by exponential extrapolation [31, 82]. These $E_{\mathrm{max}}^{\mathrm{static}}$ values in combination with the measured leakage factor values can be used to calculate an estimate of the ODNP coupling factor ξ by assuming that the saturation factor s is 1 [43, 83]. The corresponding values are listed in Table 4. These values for the coupling factors ξ are conservative estimations, as the saturation factor s is usually lower than 1. The coupling factor for water obtained in this way is about 0.12, whereas that for acetonitrile is only about 0.05; this shows again that TEMPO radicals are particularly well suited for ODNP in water. Furthermore, a temperature effect leads to a higher coupling factor of water compared to acetonitrile: the dielectric properties of water and acetonitrile are different, which leads to a substantially stronger heat uptake under microwave irradiation for water than for acetonitrile, which, in turn, leads to a higher coupling factor for water. Therefore, the difference in the isothermal

coupling factors between water and acetonitrile is likely to be smaller than suggested by the values in Table 4. In the literature, some values for static ODNP measurements of water with immobilized TEMPO systems are available for comparison, as many groups focus on aqueous systems. The Han group has worked with two different sepharose-based matrices for hyperpolarization of water [46]. The first matrix was synthesized by coupling of TEMPO radicals directly on sepharose and provided a coupling factor of 0.07 and an $E_{\mathrm{max}}^{\mathrm{static}}$ value of -42. For the second matrix, an additional polyvinylimidazole polyelectrolyte linker was used and an improved coupling factor of 0.22 was achieved and an $E_{\mathrm{max}}^{\mathrm{static}}$ value of -122 which is above the $E_{\mathrm{max}}^{\mathrm{static}}$ value obtained in the present work. The main difference is that the polyvinylimidazole linker is a polyelectrolyte, which exhibits not only a favorable interaction with water but is also present in a stretched conformation in water at pH 7, leading to improved radical-target molecule contact. However, the PEI-linker used in our systems can be easily converted in a polyelectrolyte by simply lowering the pH. PEI is essentially uncharged at about pH 7; however, upon lowering the pH the amine groups are protonated and PEI gets a positive net charge. This is expected to lead to stretched conformation [84], and hence, to an improved accessibility of the radicals.

To test this hypothesis, static ODNP-enhanced NMR measurements of water at different pHs using CPG-PEI25000-GT with pore size of 200 nm were performed. The radical matrix with the highest pore size was chosen for these experiments in order to observe the stretching effect of the PEI-linker at lower pHs undisturbed from size restrictions introduced by the pore walls. 0.2 M solution of hydrochloric acid was used for adjusting the pH in the solutions to 3, 4, 5, and 7. The results of the corresponding measurements are shown in Figure 10.

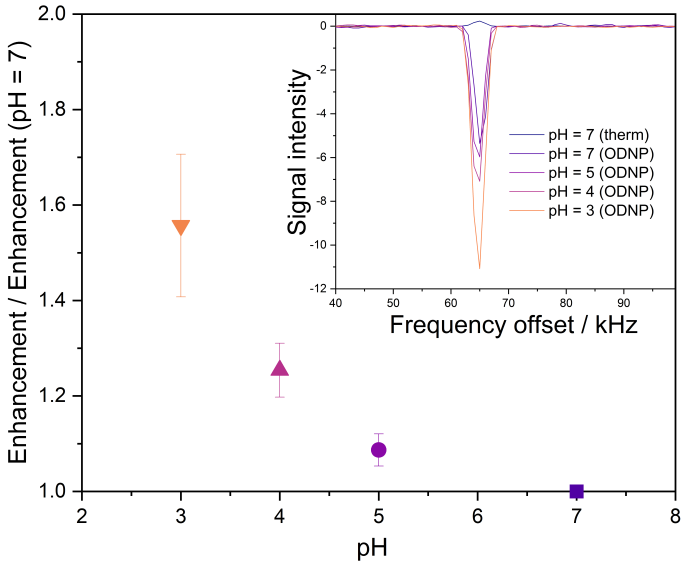

Figure 10: Results from static ODNP-enhanced ^{1}H NMR measurements of water with CPG-PEI25000-GTEMPO (pore size 200 nm) at different pH. The symbols are experimental results and were obtained as the arithmetic mean of five individual samples. The error bars indicate the standard deviation. Insert: thermally polarized (therm, acquired with 16 scans) and hyperpolarized (ODNP, single-scan) ^{1}H NMR spectra.

The hypothesis is fully confirmed by the results shown in Figure 10. Going from pH 7 to pH 3 the absolute enhancement increases by more than 50%. The enhancements measured for pH 3 was about -100 and, hence, in the range of the values achieved with sepharose-based materials that are grafted with polyvinylimmidazole [43]. Furthermore, the PEI-linker that was used in the present work was branched, which limits the positive effect of stretching on the accessibility. However, our results clearly show that CPG radical matrices tolerate acidic conditions which is not the case for sepharose-based matrices. This chemical resistance is highly beneficial for process monitoring applications.

3.4.3 Flow ODNP

The ODNP performance of the new CPGs in continuous-flow experiments with water and acetonitrile was tested. Continuous-flow ODNP experiments have the advantage, that sample heating effects are significantly reduced compared to static experiments because the irradiated sample volume is continuously exchanged. However, the microwave operation times are much longer in continuous-flow experiments than in the static experiments described before which can result in significant heating of the microwave resonator itself and a corresponding frequency drift. Thus, the microwave resonator was actively cooled with cold nitrogen gas in our continuous-flow ODNP experiments. The temperature of the ENDOR probehead was measured by a platinum resistance

thermometer and kept at about 288 K by adjusting the temperature of the nitrogen feed, which was controlled by electric heating [15]. Figure 11 shows results from continuous ODNP measurements with CPG-PEI25000-GT (pore size 50 nm) with water, in which both the microwave power and the flow-rate were varied. The highest flow-rate corresponds to a mean flow velocity of about 0.7 m s^{-1}. The corresponding results for acetonitrile are shown in the Supporting Information and confirm the trends from Figure 11.

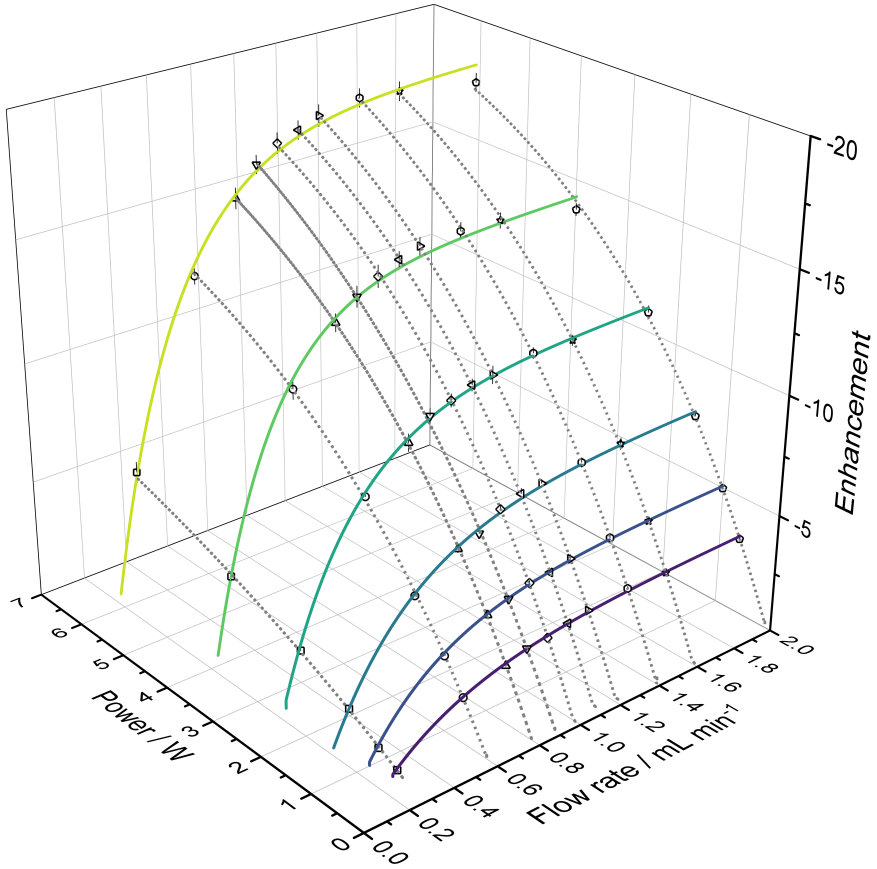

Figure 11: Results from continuous-flow ODNP measurements with water obtained with CPG-PEI25000-GT (pore size 50 nm) versus applied microwave power and flow-rate. The symbols are experimental results and were obtained as the arithmetic mean of the results of three individual samples. Solid lines: guide to the eye. Dashed lines: exponential fit [31, 82].

The signal enhancement in continuous-flow ODNP experiments was calculated from the integral of the hyperpolarized signal measured in the 1 Tesla benchtop NMR (microwave on) at a certain flow-rate relative to the integral of the thermally polarized benchtop NMR signal at a flow-rate of 0.25 mL min^{-1} (microwave off). At this flow-rate, first hyperpolarized signals were detected in continuous-flow ODNP measurements independent of applied microwave power. Thermal polarization of water in the benchtop NMR spectrometer is about three times larger than the thermal polarization in the 0.35 Tesla

Halbach magnet. Therefore, the absolute ODNP enhancement is expected to be three times lower than in the powersweep data shown in Figure 9. The enhancement values observed in flow experiments are slightly smaller than this, which is caused by polarization losses due to T_1 relaxation during the transport of the hyperpolarized water from the ODNP unit to the NMR detection site, cf. Figure 8. $E_{\mathrm{max}}^{\mathrm{static}}$ values of water were reached at a microwave power of about 6 W (cf. Figure 9 and Table 4) in the static powersweep experiments, whereas the extrapolation of the data shown in Figure 11 indicates that in continuous-flow experiments about 15 W are needed. The differences to the static powersweeps is attributed to the different saturation efficiency of the sample. Static experiments were performed in a glass microcapillary and continuous-flow experiments with a dedicated container made of PEEK to store the CPG radical matrix. In addition, coupling factors in continuous-flow ODNP are less amplified by increasing temperature during microwave irradiation.

Figure 11 shows that a large sensitivity improvement in continuous-flow benchtop NMR spectroscopy was accomplished by ODNP. This is especially important in the fast-flow regime where the thermal NMR signal almost completely vanishes due to very short prepolarization times. The overall volume in our set-up is less than 2 mL. NMR measurements were performed directly on the peek capillary resulting in a small sample volume of about 0.5 µL in the NMR coil, but still NMR spectra with very good SNR were recorded in single-scan acquisition at fast flow-rates. Finally, the long-term stability of the synthesized CPG radical matrices for continuous-flow ODNP was investigated. The radical matrices were stored in different liquids, i.e. acetone, water, diethyl ether, acetonitrile and 3-pentanone for a period of 50 days, during which the liquid supernatant was analyzed for possible radical leakage by EPR spectroscopy. No radicals were detected in any of the solvents, indicating a good long-term stability of the CPG radical matrices.

3.5 Conclusions

New CPG radical matrices for producing hyperpolarized radical-free liquids via ODNP are presented. CPGs are robust and chemically inert solid materials that can be used in process monitoring applications. The radical matrices were designed to fulfill the following requirements: sufficient radical loading for high ODNP efficiency, high mobility of radicals and good accessibility of the radicals for the target molecules, chemical inertness, temperature stability, pH stability, long-term stability, and good flow characteristics. The synthesis of the new CPGs radical matrix is simple and is accomplished in three steps by using non-hazardous chemicals. A set of six different radical matrices was synthesized by using CPGs with different pore diameters and two PEI-linkers

with different molecular masses for the immobilization of TEMPO radicals. The use of the polymeric PEI-linker is mandatory to increase the number of binding sites for the immobilization of radicals, which are too low for the commercially available CPGs. The radical loading of the synthesized matrices was measured by EPR spectroscopy and the relaxation behavior of liquids in static contact with these matrices was studied by NMR spectroscopy, allowing for the determination of the ODNP leakage factor. It was demonstrated that the radical loadings achieved with the high molecular mass PEI-linker are sufficient, with leakage factors of about 0.9. ODNP measurements dependent on microwave power were performed for acetonitrile and water in static contact with these CPG radical matrices in order to get information of the maximal possible ODNP enhancements ($E_{\mathrm{max}}^{\mathrm{static}}$) and the ODNP coupling factor ξ. The obtained $E_{\mathrm{max}}^{\mathrm{static}}$ values as well as the coupling factor ξ for water are similar to values that were obtained for sepharose-based systems known from the literature. Moreover, the obtained enhancements were substantially improved by simply by lowering the pH in measurements with water. This is attributed to the fact that the PEI-linker becomes a stretched polyelectrolyte when it is protonated, resulting in improved radical-target molecule contact, which is highly beneficial for ODNP. Our results clearly show that CPGs tolerate acidic conditions which is useful for process monitoring applications. Results from stability tests that were carried out for 50 days indicate a good long-term stability of the new CPG radical matrices in common solvents. The CPG radical matrices were also tested in continuous-flow ODNP experiments, demonstrating that they provide a large sensitivity improvement in continuous-flow benchtop NMR spectroscopy. The active volume in the NMR coil of the benchtop spectrometer is about 0.5 µL, but still satisfying NMR spectra were recorded in single-scan acquisition at fast flow-rates with ODNP. The major extension of the accessible range of flow-rates of continuous-flow benchtop NMR spectroscopy that is achieved thereby is especially important for the monitoring of very fast processes, where the residence time and volume in bypass lines have to be as small as possible to obtain a high temporal resolution. Robust CPG radical matrices were used as a fixed bed for ODNP applications, which can be easily modified to allow improved hyperpolarization of polar or nonpolar solvents by using various different polymers and radicals.

4 Quantitative Analysis in Continuous-Flow ^{1}H Benchtop NMR Spectroscopy by Paramagnetic Relaxation Enhancement

4.1 Introduction

In ^{1}H NMR spectroscopy, several seconds of residence time in the magnetic field prior NMR detection are required for efficient prepolarization. This results in a significant limitation of the monitoring application. This prepolarization problem can be tackled by the addition of paramagnetic relaxation agents to the sample which drastically shorten the T_1 of the surrounding nuclei, resulting in the so-called paramagnetic relaxation enhancement (PRE) [85–87]. The PRE effect is mainly dependent on electron-nuclear dipole-dipole interactions, which scale with distance as r^{-6} [88]. Many different PRE agents have been developed based on either stable radicals or metal complexes. They can roughly be divided in two categories: dissolved paramagnetic materials and immobilized paramagnetic materials. A major application field of PRE NMR is medical imaging, where dissolved metal complexes, based on e.g. gadolinium (III) ions are used as contrast agents [18, 89–92]. These metal complexes are usually optimized for most efficient relaxation of water protons and yield only poor PRE efficiencies in nonpolar solvents, which reduces their applicability in process monitoring applications.

Furthermore, dissolved paramagnetic material in the sample can hamper NMR detection, because it has an influence not only on the T_1 of the molecules but also on their transversal relaxation time T_2, which can lead to an undesired broadening of the NMR lines. This is especially disturbing if the PRE agent is used in high concentrations for maximizing its effect or in continuous-flow NMR applications, where an additional broadening of NMR lines is observed due to out-flow effects of the sample during NMR

acquisition [93]. It is therefore advantageous to use a fixed bed of PRE agent instead, through which the sample passes before entering the NMR coil for detection [15, 20, 94]. Immobilized free radicals (IFRs) were already used in the early 1980s to shorten T_1 of ^{1}H nuclear spins. In addition, immobilized and dissolved PRE agents were studied in continuous-flow high field NMR with heteronuclear detection [21, 95]. Moreover, it has been demonstrated that a larger linker, and hence a greater distance from the surface of the carrier material, can result in an improved PRE [40]. However, the radical loading of PRE agents must be high enough to ensure a T_1 reduction sufficient for enabling quantitative flow NMR in the short polarization length of benchtop NMR spectrometers. Thus, new synthesis strategies are required to achieve high radical loadings of PRE agents. Moreover, for process and reaction monitoring applications it is mandatory that the PRE agent is compatible with polar and nonpolar solvents. Additionally, it should be robust, chemically inert, and exhibit a good long-term stability.

In the present work, a new PRE agent that matches the above-mentioned design criteria was developed that was again based on PEI-grafted CPGs with a branched PEI-linker and GT. Its PRE efficiency should be high enough to ensure complete ^{1}H polarization buildup in benchtop NMR spectrometers even at high flow velocities. Therefore, a fixed bed of a solid PRE agent with high radical loading was synthesized and applied in quantitative continuous-flow benchtop ^{1}H NMR spectroscopy. Aminopropyl-grafted controlled porous glass (CPG) was used as solid support material because of its high chemical inertness and good flow characteristics. Polyethyleneimine was first coupled to the CPG to multiply the binding sites for the coupling of nitroxide radicals [96] in order to achieve a sufficiently high radical loading. Thereafter, glycidyloxy-tetramethylpiperidinyloxyl (GT) radicals were coupled to the binding sites of the polymer. To examine the PRE effect of the synthesized material, several liquids commonly used as solvents in industrial processes, were investigated with respect to their polarization buildup in contact with the synthesized PRE agent. Furthermore, two binary mixtures (acetonitrile+water and acetonitrile+1,4-dioxane) were studied in quantitative continuous-flow ^{1}H NMR experiments with varying flow velocities to demonstrate a sufficient PRE efficiency of the new material.

4.2 Materials and Methods

Chemicals used in the presented synthesis and in continuous-flow benchtop NMR are listed in Table 5 and were used without further purification. Water was obtained using an Elix Essential 5 purification system from Merck.

Table 5: Chemicals used in the presented synthesis and in continuous-flow NMR experiments are listed with respective suppliers and purities.

Chemical	Supplier	Purity / g g^{-1}
Aminopropyl-CPG	Biosearch Technologies	
GT	TCI	> 0.950
1,4-Butanediol diglycidyl ether	Sigma Aldrich	> 0.950
Polyethyleneimine	Sigma Aldrich	> 0.990
Methanol	Sigma Aldrich	≥ 0.999
Ethanol	Sigma Aldrich	≥ 0.999
Acetonitrile	Roth	≥ 0.999
Acetone	Sigma Aldrich	≥ 0.998
Ethylene glycol	Roth	≥ 0.995
Benzonitrile	Sigma Aldrich	≥ 0.998
1-Propanol	Sigma Aldrich	≥ 0.995
2-Propanol	Sigma Aldrich	≥ 0.999
Tetrahydrofuran	Sigma Aldrich	≥ 0.999
Pyridine	Fisher Scientific	≥ 0.999
1,4-Dioxane	Sigma Aldrich	≥ 0.998

Aminopropyl-CPGs (350 mg) with a pore size of 30 nm were added to ethanol (5×2.0 mL) and centrifuged (5 min at 2500 rpm). 1,4-Butanediol diglcyidyl ether (283.15 mg) was dissolved in methanol (3.5 mL) and dry aminopropyl-CPGs were added. The reaction mixture was rotated in a tube rotator for 24 h at room temperature. Water (5×15 mL) and later ethanol (2×15 mL) was added and centrifuged (5 min at 2500 rpm). Polyethyleneimine (molecular mass of 25 000 g mol^{-1}, 8.75 g, 20 mM) was dissolved in methanol and BDGE-grafted CPGs were added. The reaction mixture was rotated in a tube rotator for 24 h at room temperature. Water (5 × 15 mL) and later ethanol (2 × 15 mL) were added and centrifuged (5 min at 2500 rpm). GT (399.56 mg, 0.5 mM) was dissolved in methanol and added to previously prepared PEI-grafted CPGs. The reaction mixture was rotated in a tube rotator for 24 h at room temperature. Water (5 × 15 mL) was added and CPGs were separated by filtration. The product was stored in water (2.0 mL) at 277 K.

Radical loading of the synthesized PRE agent was studied with a MicroESR-X-Band spectrometer from Bruker. Analysis was performed using micro capillaries from Blaubrand intraMark with an inner diameter of 1 mm and a sample volume of around 4 µL. Samples were sealed with Leica Microsystems Critoseal capillary tube sealant. The concentration of immobilized radicals was determined by comparison of EPR integrals with aqueous solutions of dissolved GT. Acquisition parameters were set to: microwave

power 15 mW, modulation coil amplitude 1.0 G, and receiver gain 12 dB; and an average of 16 scans was used [96].

A benchtop NMR spectrometer (Spinsolve Carbon, manufactured by Magritek) operating at a proton resonance frequency of 43 MHz was used for all NMR experiments. Inversion recovery NMR measurements were performed in microprobe NMR tubes purchased from Norell with an outer diameter of 2.5 mm, which were used to minimize the sample volume. For samples in static contact with the synthesized PRE agent, the supernatant was removed several times after brief centrifugation, so that finally no liquid without static contact with the PRE agent was in the active volume of the NMR spectrometer. Parameters were set with the standard T_1 measurement protocol supplied by Magritek. The relaxation delay between several excitations was chosen to be sufficiently high for complete equilibration of the nuclear spins. An average of 8 scans was used. The relative error of calculated T_1 values from successive NMR measurements is less than 1% in this work.

Benchtop ^{1}H NMR spectroscopy with PRE agent was performed with a container manufactured of Polyether ether ketone (PEEK) that was positioned directly in front of the NMR-active volume of the benchtop NMR spectrometer to store the PRE agent [15]. Inner diameter of this PEEK container and of the PEEK capillary running through the benchtop NMR spectrometer was 1 mm. 300 mg of PRE agent was filled in the PEEK container, which results in a filling height of around 50 mm. Samples were fed to the set-up using a HPLC pump purchased from Flusys that was additionally equipped with a mass flow meter (Mini CORI-FLOW) purchased from Bronkhorst. NMR experiments were performed with short acquisition times of around 400 ms. The recycle delay between individual scans was set to 3 s, which ensured a full exchange of the liquid in the active volume of the RF coil. The standard deviation in successive continuous-flow NMR data is overall less than 2% in this work. NMR data without flow was recorded with a recycle delay of 30 s.

4.3 Results and Discussion

4.3.1 Continuous-Flow Benchtop ^{1}H NMR Spectroscopy without PRE Agent

In benchtop ^{1}H NMR experiments, the problem of incomplete polarization buildup occurs already at moderate flow velocities. This is illustrated in Figure 12 by results calculated with Equation 1 for a polarization length of 0.1 m typical for benchtop NMR spectrometers, for 12 common solvents based on the T_1 values given in Table 6. For

molecules with several distinguishable protons, the highest T_1 was used. In addition, experimental results are presented for water using a PEEK capillary with 1 mm inner diameter, which was simply inserted into the bore of the flow probe. Experimental data is shown as squares and was obtained as the arithmetic mean value of three individual NMR acquisitions. As can be seen in Figure 12, they agree very well with the predictions based on Equation 1.

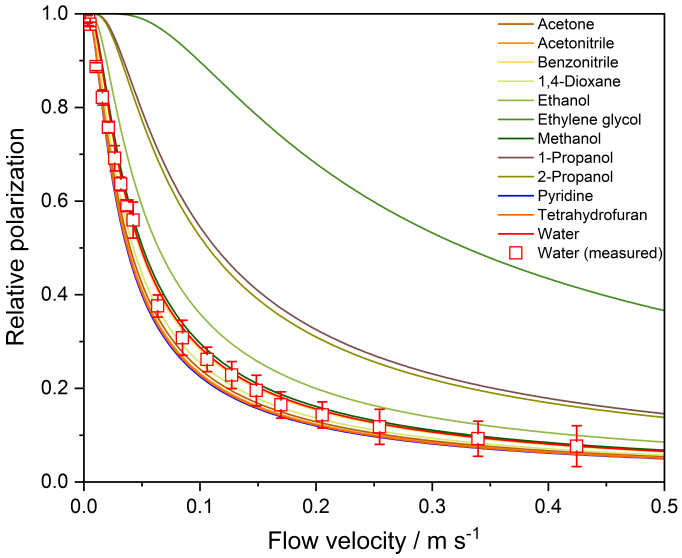

Figure 12: Relative polarization of protons of 12 common solvents versus flow velocity. Lines represent calculations using Equation 1. Squares are experimental results for water measured in a 1 Tesla benchtop NMR spectrometer and were obtained as the arithmetic mean of three individual acquisitions. Error bars indicate the standard deviation.

Table 6: Overview of measured longitudinal relaxation times T_1 of common solvents at 1 Tesla and 301.7 K. For molecules with several distinguishable protons, the highest T_1 is listed. T_1^{RM} denotes measured values of the investigated solvents in static contact with the synthesized PRE agent.

Solvent	T_1 / s	T_1^{RM} / s	PRE $(T_1\text{-}T_1^{RM})/T_1$
Water	3.10	0.05	0.98
Acetonitrile	3.99	0.05	0.99
Ethanol	2.36	0.06	0.97
Ethylene glycol	0.46	0.12	0.74
Benzonitrile	3.16	0.06	0.98
Acetone	3.82	0.13	0.97
Methanol	2.99	0.15	0.95
1-Propanol	1.34	0.16	0.88
2-Propanol	1.42	0.17	0.88
Tetrahydrofuran	4.07	0.19	0.95
Pyridine	4.13	0.09	0.98
1,4-Dioxane	3.58	0.21	0.94

Figure 12 shows that already moderate flow velocities well below 0.1 m s^{-1} generally result in drastic polarization losses in continuous-flow benchtop ^{1}H NMR applications without PRE agents. The relative polarization decreases exponentially with increasing flow velocity, corresponding to around 80-90% signal loss at a flow velocity of 0.4 m s^{-1} for most of the studied solvents. The decrease in relative polarization is most pronounced for solvents with long T_1. However, bringing the solvents in contact with a PRE agent drastically shortens their T_1 (denoted as T_1^{RM} in Table 6) and greatly accelerates the polarization buildup.

4.3.2 Continuous-Flow Benchtop ^{1}H NMR Spectroscopy with PRE Agent

4.3.2.1 Synthesis of New PRE Agent

Controlled porous glasses (CPGs) were chosen as solid support material of the PRE agent because they are robust, chemically inert, exhibit a good flow characteristic, and are commercially available in high quality. In this work, aminopropyl-functionalized CPG with a pore size of 30 nm and particle size of 70 to 140 µm were used, which possesses a high surface area, and, thus, a high number of binding sites. However, direct coupling of GT on the CPG resulted in an immobilized radical concentration of only 1.5 mM, which is far too low for a high PRE efficiency with CPG-based materials

[96]. Therefore, the number of available binding sites had to be significantly increased, which was achieved by first coupling a cross-linked polymer exhibiting many binding sites (polyethyleneimine, PEI) to the CPG before attaching the stable nitroxide radical GT. Solid fixed beds of this type were synthesized for hyperpolarized NMR by Overhauser dynamic nuclear polarization (ODNP), where immobilized free electrons are also essential. For ODNP-enhanced NMR, the aim was to achieve radical loadings in the range of 20 to 30 mM [96]. Here, our aim was to further increase the concentration of radicals to optimize their PRE efficiency. The synthesis of the new PRE agent is shown in a simplified scheme in Figure 13. The CPG has multiple aminopropyl groups on the surface and in the pores, but, for simplicity, Figure 13 shows only one of these binding sites of the CPG.

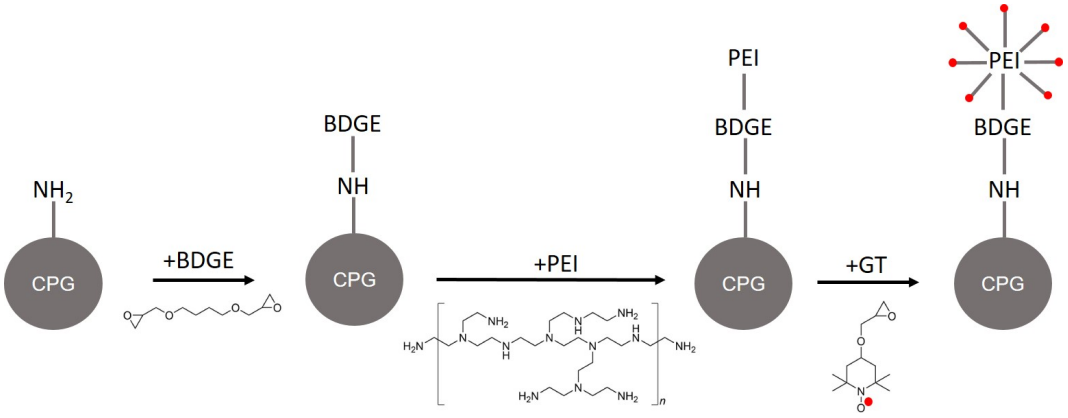

Figure 13: Scheme of the three-step synthesis of the new PRE agent: (1) coupling of BDGE on aminopropyl-functionalized CPGs; (2) coupling of PEI on BDGE-grafted CPGs; (3) immobilization of GT on PEI-grafted CPGs. All reactions are solely performed in methanol at ambient temperature.

Figure 13 shows that the coupling reactions in the presented immobilization procedure of GT take place exclusively via the reaction of epoxy and amino groups in all three synthesis steps. This is a selective reaction that can be carried out under mild conditions. Here, reactions were solely performed at 293 K in methanol for a period of 24 h, which resulted in a stable radical concentration of 120 mM in the synthesized paramagnetic fixed bed. The paramagnetic fixed bed showed no degradation in the entire series of continuous-flow experiments.

In order to analyze the PRE efficiency of the synthesized material, T_1 of 12 common solvents was measured in static contact with the synthesized PRE agent (T_1^{RM}) and without the PRE agent. Table 6 lists T_1 of investigated solvents, which were measured directly in the benchtop NMR spectrometer. The experimental results were obtained as the arithmetic mean of the results of three individual measurements. T_1 of the studied solvents was reduced by at least 74% in contact with the PRE agent, and for most

solvents significantly more, e.g. the T_1 for water and acetonitrile was reduced by 98% to 50 ms in static contact with the PRE agent. For most of the solvents, the PRE efficiency is around 90%, which is remarkable because the solvents exhibit different polarities. Only for molecules with a rather short native T_1 is the PRE efficiency reduced, because here other relaxation pathways are involved, which reduce the possible paramagnetic relaxation. All solvents show T_1^{RM} values in contact with the radical matrix of less than 200 ms, which significantly shortens the time required for complete polarization buildup.

4.3.2.2 Experimental Set-up

For demonstrating the applicability of the new PRE agent in continuous-flow benchtop NMR spectroscopy, quantitative ^{1}H NMR measurements were performed at different flow velocities. The corresponding set-up with incorporated PRE agent is shown in Figure 14. The liquid to be analyzed first passes through a fixed bed of the PRE agent where the accelerated polarization buildup takes place before entering the NMR-active volume.

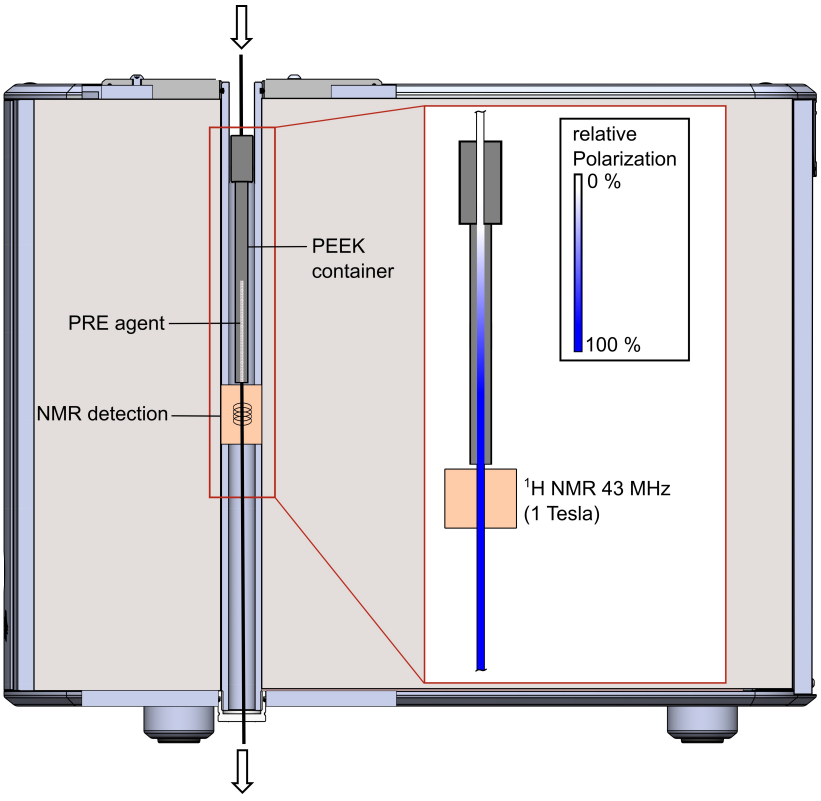

Figure 14: Set-up for continuous-flow benchtop NMR spectroscopy with PRE agent. The direction of the liquid flow is indicated by arrows. Insert: visualization of accelerated polarization buildup in the flow path with PRE agent.

Data were always acquired with a 1 Tesla benchtop NMR spectrometer from Magritek (Spinsolve Carbon, proton frequency of 43 MHz), into which a 1 mm inner-diameter

PEEK capillary containing the flowing liquid sample was placed. The PRE agent was installed in a PEEK container with 1 mm inner diameter positioned directly prior the NMR coil in the flow path. NMR experiments were performed with acquisition times of 400 ms to minimize out-flow effects that occur when the sample is already leaving the active volume of the NMR spectrometer during acquisition.

4.3.2.3 Polarization in Continuous-Flow Benchtop ^{1}H NMR Spectroscopy

To demonstrate the effect of the PRE agent on the prepolarization buildup, ^{1}H NMR measurements with and without PRE agent were compared. Measurements were performed on two binary liquid systems (system 1: acetonitrile+water and system 2: acetonitrile+1,4-dioxane) of different compositions with the experimental set-up shown in Figure 14.

Figure 15 shows the results of the recorded signal integral of acetonitrile for four different compositions of system 1 (acetonitrile+water) at flow velocities up to 0.04 m s^{-1}. Figure 16 shows the results for water in system 1. The presented results were obtained from three individual acquisitions, where the recorded signal integral was normalized by dividing it by the number of protons in the studied functional group. Error bars (smaller than symbol size) indicating standard deviation are not shown for clarity purposes.

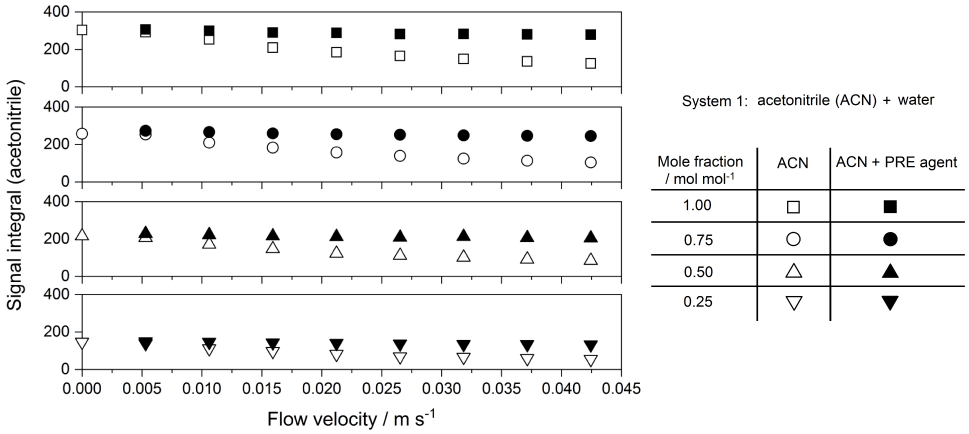

Figure 15: Comparison of ^{1}H NMR signal integrals of acetonitrile (ACN) for mixtures in system 1 (acetonitrile+water) recorded with the benchtop NMR spectrometer (open symbols) and with installed PRE agent (closed symbols). Symbols are experimental results and were obtained as the arithmetic mean value of three individual acquisitions.

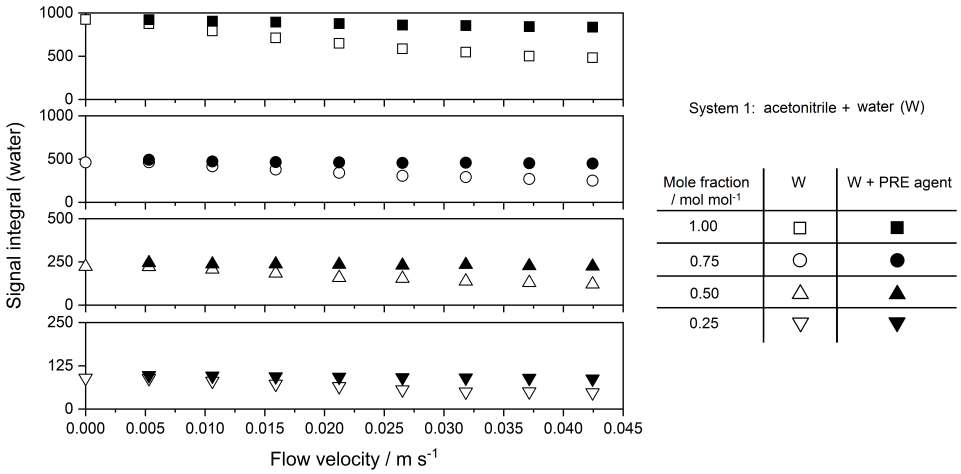

Figure 16: Comparison of ^{1}H NMR signal integrals of water (W) for mixtures in system 1 (acetonitrile+water) recorded with the benchtop NMR spectrometer (open symbols) and with installed PRE agent (closed symbols). Symbols are experimental results and were obtained as the arithmetic mean value of three individual acquisitions. The scale of the signal integral for compositions with mole fractions of water ≤ 0.50 mol mol^{-1} is increased.

The signal integrals of acetonitrile and water decrease significantly with increasing flow velocity without PRE agent. At a flow velocity of 0.04 m s^{-1} signal integrals of acetonitrile are reduced by around 50% for all studied mixtures without PRE agent compared to the signal without flow. The signal integrals of water were reduced by around 40% due to the shorter T_1 of water. In addition, as the concentration of water in the mixture decreases, the polarization problem of the water protons becomes less severe. Low concentrations of water in this binary system result in shorter T_1 of water [39], which slightly improves the buildup of its polarization.

This trend can also be observed in the measurements with PRE agent. For water, the signal integral is almost stable over the examined flow velocity range at a comparable value to the measurement without flow. The reduction of the signal integrals for both components at the highest studied flow-rate is less than 10%. However, a small decrease in signal for both components with increasing flow velocity can still be observed, although the polarization buildup must be complete given the short T_1^{RM} of water and acetonitrile in contact with the PRE agent. This small drop in signal integrals can be attributed to out-flow effects. Nevertheless, signals for both components can be maintained at values comparable to data measured without flow over the entire velocity range.

Figures 17 and Figure 18 show the results of the same experiments for system 2 (acetonitrile+1,4-dioxane).

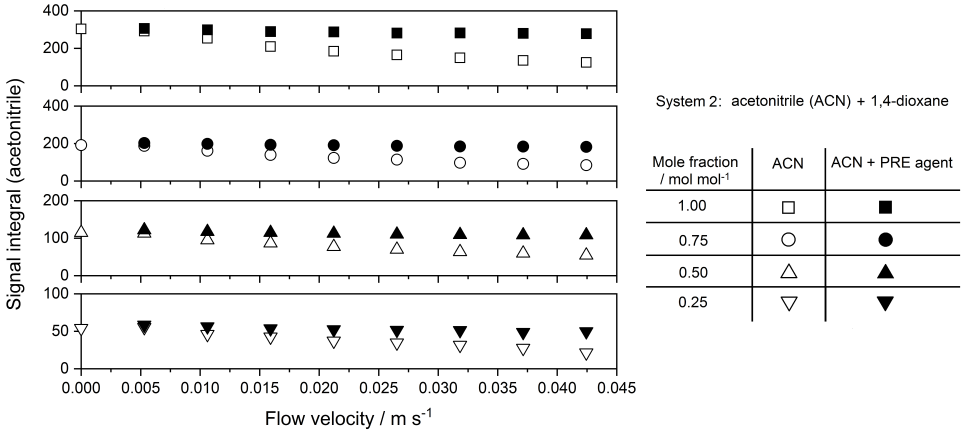

Figure 17: Comparison of ^{1}H NMR signal integrals of acetonitrile (ACN) for mixtures in system 2 (acetonitrile+1,4-dioxane) recorded with the benchtop NMR spectrometer (open symbols) and with installed PRE agent (closed symbols). Symbols are experimental results and were obtained as the arithmetic mean value of three individual acquisitions. The scale of the signal integral for compositions with mole fractions of acetonitrile ≤ 0.50 mol mol^{-1} is increased.

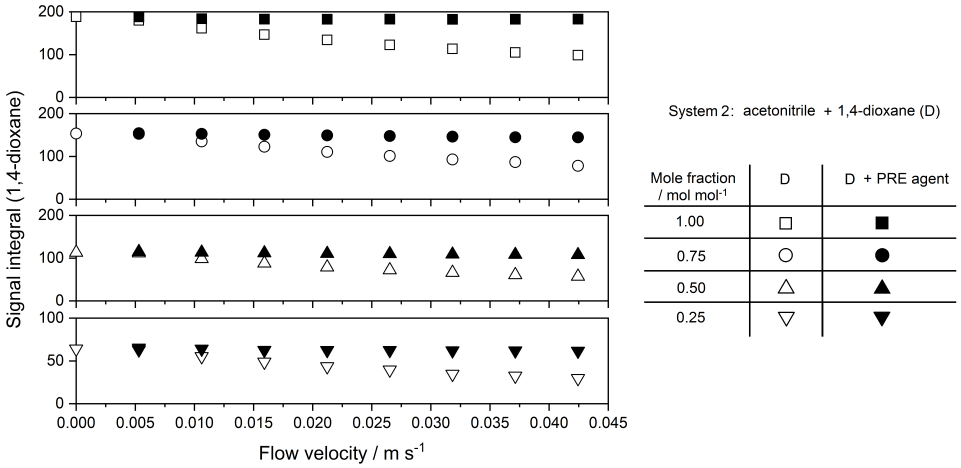

Figure 18: Comparison of ^{1}H NMR signal integrals of 1,4-dioxane (D) for mixtures in system 2 (acetonitrile+1,4-dioxane) recorded with the benchtop NMR spectrometer (open symbols) and with installed PRE agent (closed symbols). Symbols are experimental results and were obtained as the arithmetic mean value of three individual acquisitions. The scale of the signal integral for the composition with a mole fraction of 1,4-dioxane of 0.25 mol mol^{-1} is increased.

The results recorded with the benchtop NMR spectrometer without PRE agent show again an ineffective polarization buildup for both components. The signal of acetonitrile is reduced by around 60% at a flow velocity of 0.04 m s^{-1} for all studied concentrations and for 1,4-dioxane by around 50% compared to the respective signal without flow. By using the PRE agent, the signal integral was comparable to the signal without flow and therefore exhibited high SNR in the ^{1}H NMR spectrum for both components at all

studied flow velocities. The small signal decrease that is still observable in the measurements with PRE agent is again caused by out-flow effects during NMR acquisition and is not due to incomplete polarization buildup in this range of flow velocities.

4.4 Quantification in Continuous-Flow Benchtop ^{1}H NMR Spectroscopy

Figure 19 and Figure 20 show the results of the quantitative analysis of continuous-flow measurements with and without the PRE agent. Open symbols represent the results without the PRE agent, whereas closed symbols indicate the results with the PRE agent. The dashed lines in the figures represent the ground truth, which corresponds to the mole fractions of the original sample weight. To calculate the mole fraction, the signal integrals shown in Figure 15 to Figure 18 were normalized by dividing each signal integral by the sum of the signal integrals of both components present in the mixture. Calculated mole fractions are shown for three compositions of the studied systems, c.f. Figure 19 for system 1 (acetonitrile+water) and Figure 20 for system 2 (aceontrile+1,4-dioxane).

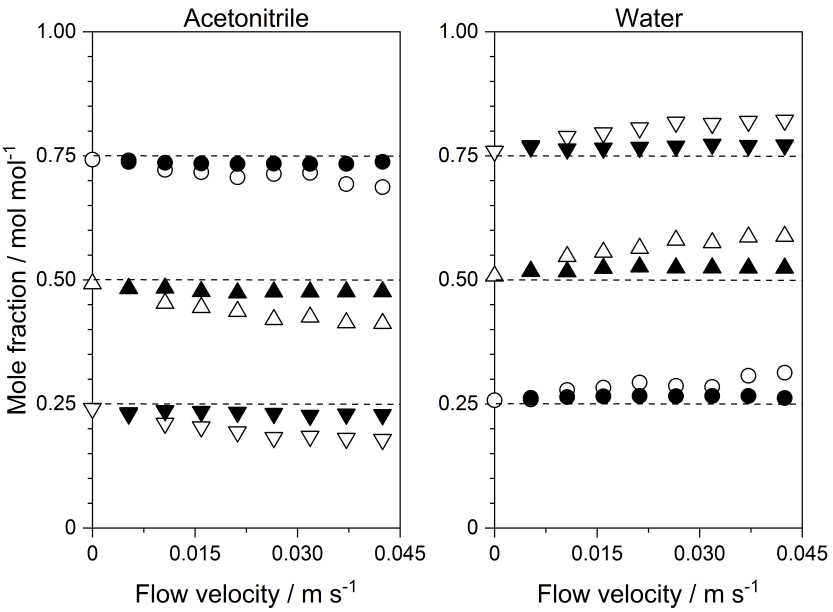

Figure 19: Quantification of ^{1}H NMR data for system 1 (acetonitrile+water). Left panel: acetonitrile mole fractions, right panel: water mole fractions. Dashed lines represent the mole fraction of the original sample weight of the prepared mixtures. Open symbols show data for the benchtop NMR set-up without PRE agent. Closed symbols show data for the presented set-up with PRE agent.

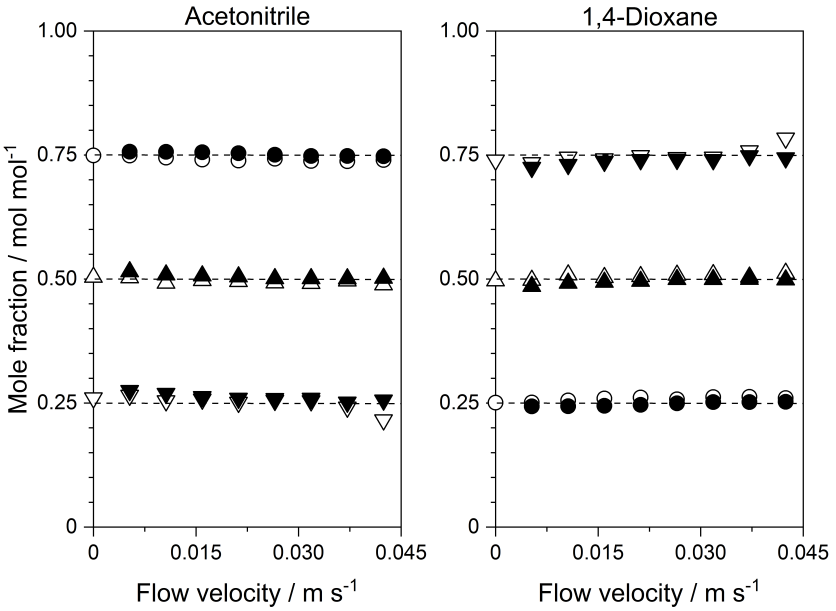

Figure 20: Quantification of ^{1}H NMR data for system 2 (acetonitrile+1,4-dioxane). Left panel: acetonitrile mole fractions, right panel: 1,4-dioxane mole fractions. Dashed lines represent the mole fraction of the original sample weight of the prepared mixtures. Open symbols show data for the benchtop NMR set-up without PRE agent. Closed symbols show data for the presented set-up with PRE agent.

In quantitative ^{1}H NMR measurements performed with PRE agent, a higher quantification accuracy of the ground truth of the prepared mixture was achieved compared to measurements without PRE agent for both systems in the entire velocity range. In Figure 19, measurements without PRE agent showed a relative error of around 11% in the quantification of the mole fractions of acetonitrile and water for all compositions and flow velocities in system 1, whereas the relative error is severely reduced in measurement with PRE agent to about 4.5%. Figure 20 shows that there is only a small difference in quantification with and without PRE agent in system 2 in the studied range of flow velocities: i.e. without PRE agent the relative error was around 1.7%, whereas the relative error is reduced in measurements with PRE agent to about 1.5%. In system 2, the T_1 of both components is similar, which leads to almost the same decrease in the recorded NMR signal for both substances (c.f. Figure 17 and Figure 18). However, for systems with a slightly larger difference in T_1 this is not the case, resulting in inaccurate quantification as can be seen from the evaluation of system 1.

4.5 Conclusions

A new immobilized PRE agent for improved paramagnetic relaxation in continuous-flow benchtop NMR spectroscopy was synthesized and tested. The PRE agent was synthe-

sized using controlled porous glass particles with a pore size of 30 nm. By grafting the CPG surface with butanediol diglycidyl ether and polyethyleneimine, the binding sites available for immobilizing the nitroxide radical TEMPO were multiplied. The resulting PRE agent with a radical loading of 120 mM shows a high PRE efficiency and no degradation in the entire series of experiments. The new PRE agent was tested in continuous-flow benchtop ^{1}H NMR experiments at flow velocities for which significant signal loss of 50-70% occurs when no PRE agent is used. The results show that accelerated polarization buildup occurs over the whole studied velocity range with application of the PRE agent. Using the PRE agent clearly improved the results of quantification in cases where components in the mixture had different T_1. Thus, the new PRE agent is useful for applications in reaction and process monitoring with benchtop NMR spectrometers. Future work will focus on the application of the new PRE agent for the improved detection of heteronuclei (such as ^{13}C) in process engineering applications.

Literature

[1] M. Goldbach, E. Danieli, J. Perlo, B. Kaptein, V. M. Litvinov, B. Blümich, F. Casanova, A. L. Duchateau: Preparation of grignard reagents from magnesium metal under continuous flow conditions and on-line monitoring by NMR spectroscopy, Tetrahedron Letters 57 (2016) 122–125.

[2] A. Friebel, E. von Harbou, K. Münnemann, H. Hasse: Reaction monitoring by benchtop NMR spectroscopy using a novel stationary flow reactor setup, Industrial and Engineering Chemistry Research 58 (2019) 18125–18133.

[3] P. Giraudeau, F.-X. Felpin: Flow reactors integrated with in-line monitoring using benchtop NMR spectroscopy, Reaction Chemistry & Engineering 3 (2018) 399–413.

[4] D. A. Foley, E. Bez, A. Codina, K. L. Colson, M. Fey, R. Krull, D. Piroli, M. T. Zell, B. L. Marquez: NMR flow tube for online NMR reaction monitoring, Analytical Chemistry 86 (2014) 12008–12013.

[5] F. Dalitz, L. Kreckel, M. Maiwald, G. Guthausen: Quantitative medium-resolution NMR spectroscopy under non-equilibrium conditions, studied on the example of an esterification reaction, Applied Magnetic Resonance 45 (2014) 411–425.

[6] H.-Y. Yu, S. Myoung, S. Ahn: Recent applications of benchtop nuclear magnetic resonance spectroscopy, Magnetochemistry 7 (2021) 121.

[7] T. Castaing-Cordier, D. Bouillaud, J. Farjon, P. Giraudeau: Chapter four - recent advances in benchtop nmr spectroscopy and its applications, volume 103 of *Annual Reports on NMR Spectroscopy*, Academic Press, 2021, pp. 191–258.

[8] L. L. Wald, P. C. McDaniel, T. Witzel, J. P. Stockmann, C. Z. Cooley: Low-cost and portable MRI, Journal of Magnetic Resonance Imaging 52 (2019) 686–696.

[9] T. A. Beek: Low-field benchtop NMR spectroscopy: status and prospects in natural product analysis, Phytochemical Analysis (2020).

[10] C. Z. Cooley, J. P. Stockmann, B. D. Armstrong, M. Sarracanie, M. H. Lev, M. S. Rosen, L. L. Wald: Two-dimensional imaging in a lightweight portable MRI scanner without gradient coils, Magnetic Resonance in Medicine 73 (2014) 872–883.

[11] T. Guallart-Naval, J. M. Algarín, R. Pellicer-Guridi, F. Galve, Y. Vives-Gilabert, R. Bosch, E. Pallás, J. M. González, J. P. Rigla, P. Martínez, F. J. Lloris, J. Borreguero, Á. Marcos-Perucho, V. Negnevitsky, L. Martí-Bonmatí, A. Ríos, J. M. Benlloch, J. Alonso: Portable magnetic resonance imaging of patients indoors, outdoors and at home, Scientific Reports 12 (2022).

[12] F. Dalitz, M. Cudaj, M. Maiwald, G. Guthausen: Process and reaction monitoring by low-field NMR spectroscopy, Progress in Nuclear Magnetic Resonance Spectroscopy 60 (2012) 52–70.

[13] G. Krüger, A. Birke, R. Weiss: Nuclear magnetic resonance (NMR) two-phase mass flow measurements, Flow Measurement and Instrumentation 7 (1996) 25–37.

[14] N. Zientek, K. Meyer, S. Kern, M. Maiwald: Quantitative online NMR spectroscopy in a nutshell, Chemie Ingenieur Technik 88 (2016) 698–709.

[15] R. Kircher, H. Hasse, K. Münnemann: High flow-rate benchtop nmr spectroscopy enabled by continuous overhauser DNP, Analytical Chemistry 93 (2021) 8897–8905.

[16] J. F. Haw, T. E. Glass, D. W. Hausler, E. Motell, H. C. Dorn: Direct coupling of a liquid chromatograph to a continuous flow hydrogen nuclear magnetic resonance detector for analysis of petroleum and synthetic fuels, Analytical Chemistry 52 (1980) 1135–1140.

[17] M. C. McIvor: A flow probe for nuclear magnetic resonance spectroscopy, Journal of Physics E: Scientific Instruments 2 (1969) 292–293.

[18] R. B. Lauffer: Paramagnetic metal complexes as water proton relaxation agents for NMR imaging: theory and design, Chemical Reviews 87 (1987) 901–927.

[19] H. H. Fischer, M. Seiler, T. S. Ertl, U. Eberhardinger, H. Bertagnolli, H. Schmitt-Willich, K. Albert: Quantification studies in continuous-flow13c nuclear magnetic resonance spectroscopy by use of immobilized paramagnetic relaxation agents, The Journal of Physical Chemistry B 107 (2003) 4879–4886.

[20] D. Bruck, R. Dudley, C. Fyfe, J. V. Delden: Sample magnetization using immobilized free radicals for use in flow NMR systems, Journal of Magnetic Resonance (1969) 42 (1981) 51–59.

[21] Y. Zhang, D. A. Laude: Immobilized free-radical substrates for magnetization of carbon-13 nuclei in flow NMR measurements, Journal of Magnetic Resonance (1969) 87 (1990) 46–55.

[22] K. Münnemann, H. W. Spiess: The art of signal enhancement, Nature Physics 7 (2011) 522–523.

[23] J. Natterer, J. Bargon: Parahydrogen induced polarization, Progress in Nuclear Magnetic Resonance Spectroscopy 31 (1997) 293–315.

[24] C. R. Bowers, D. P. Weitekamp: Parahydrogen and synthesis allow dramatically enhanced nuclear alignment, Journal of the American Chemical Society 109 (1987) 5541–5542.

[25] S. Appelt, A. B.-A. Baranga, C. J. Erickson, M. V. Romalis, A. R. Young, W. Happer: Theory of spin-exchange optical pumping of3heand129xe, Physical Review A 58 (1998) 1412–1439.

[26] T. G. Walker, W. Happer: Spin-exchange optical pumping of noble-gas nuclei, Reviews of Modern Physics 69 (1997) 629–642.

[27] T. R. Carver, C. P. Slichter: Experimental verification of the overhauser nuclear polarization effect, Physical Review 102 (1956) 975–980.

[28] J. H. Ardenkjaer-Larsen, B. Fridlund, A. Gram, G. Hansson, L. Hansson, M. H. Lerche, R. Servin, M. Thaning, K. Golman: Increase in signal-to-noise ratio of > 10,000 times in liquid-state NMR, Proceedings of the National Academy of Sciences 100 (2003) 10158–10163.

[29] F. A. Gallagher, M. I. Kettunen, S. E. Day, D.-E. Hu, J. H. Ardenkjær-Larsen, R. in 't Zandt, P. R. Jensen, M. Karlsson, K. Golman, M. H. Lerche, K. M. Brindle: Magnetic resonance imaging of pH in vivo using hyperpolarized 13c-labelled bicarbonate, Nature 453 (2008) 940–943.

[30] T. J. Keller, A. J. Laut, J. Sirigiri, T. Maly: High-resolution overhauser dynamic nuclear polarization enhanced proton NMR spectroscopy at low magnetic fields, Journal of Magnetic Resonance 313 (2020) 106719.

[31] K. H. Hausser, D. Stehlik: Dynamic nuclear polarization in liquids, Advances in Magnetic and Optical Resonance 3 (1968) 79–139.

[32] J. M. Franck, A. Pavlova, J. A. Scott, S. Han: Quantitative cw overhauser effect dynamic nuclear polarization for the analysis of local water dynamics, Progress in Nuclear Magnetic Resonance Spectroscopy 74 (2013) 33–56.

[33] E. Ravera, C. Luchinat, G. Parigi: Basic facts and perspectives of overhauser DNP NMR, Journal of Magnetic Resonance 264 (2016) 78–87.

[34] R. Gitti, C. Wild, C. Tsiao, K. Zimmer, T. E. Glass, H. C. Dorn: Solid/liquid intermolecular transfer of dynamic nuclear polarization. enhanced flowing fluid proton NMR signals via immobilized spin labels, Journal of the American Chemical Society 110 (1988) 2294–2296.

[35] H. Dorn, J. Wang, L. Allen, D. Sweeney, T. Glass: Flow dynamic nuclear polarization, a novel method for enhancing NMR signals in flowing fluids, Journal of Magnetic Resonance (1969) 79 (1988) 404–412.

[36] H. Dorn, R. Gitti, K. Tsai, T. Glass: The flow transfer of a bolus with 1h dynamic nuclear polarization from low to high magnetic fields, Chemical Physics Letters 155 (1989) 227–232.

[37] K. Halbach: Design of permanent multipole magnets with oriented rare earth cobalt material, Nuclear Instruments and Methods 169 (1980) 1–10.

[38] H. Raich, P. Blümler: Design and construction of a dipolar halbach array with a homogeneous field from identical bar magnets: NMR mandhalas, Concepts in Magnetic Resonance Part B: Magnetic Resonance Engineering 23B (2004) 16–25.

[39] A. Friebel, T. Specht, E. von Harbou, K. Münnemann, H. Hasse: Prediction of flow effects in quantitative NMR measurements, Journal of Magnetic Resonance 312 (2020) 106683.

[40] H. C. Dorn, T. E. Glass, R. Gitti, K. H. Tsai: Transfer of1h and13c dynamic nuclear polarization from immobilized nitroxide radicals to flowing liquids, Applied Magnetic Resonance 2 (1991) 9–27.

[41] S. Stevenson, T. Glass, H. C. Dorn: 13c dynamic nuclear polarization: an alternative detector for recycled-flow NMR experiments, Analytical Chemistry 70 (1998) 2623–2628.

[42] E. R. McCarney, B. D. Armstrong, M. D. Lingwood, S. Han: Hyperpolarized water as an authentic magnetic resonance imaging contrast agent, Proceedings of the National Academy of Sciences 104 (2007) 1754–1759.

[43] M. D. Lingwood, T. A. Siaw, N. Sailasuta, B. D. Ross, P. Bhattacharya, S. Han: Continuous flow overhauser dynamic nuclear polarization of water in the fringe field of a clinical magnetic resonance imaging system for authentic image contrast, Journal of Magnetic Resonance 205 (2010) 247–254.

[44] S. Ebert, A. Amar, C. Bauer, M. Kölzer, P. Blümler, H. W. Spiess, D. Hinderberger, K. Münnemann: A mobile DNP polarizer for continuous flow applications, Applied Magnetic Resonance 43 (2012) 195–206.

[45] O. Neudert, D. G. Zverev, C. Bauer, P. Blümler, H. W. Spiess, D. Hinderberger, K. Münnemann: Overhauser DNP and EPR in a mobile setup: Influence of magnetic field inhomogeneity, Applied Magnetic Resonance 43 (2012) 149–165.

[46] E. R. McCarney, S. Han: Spin-labeled gel for the production of radical-free dynamic nuclear polarization enhanced molecules for NMR spectroscopy and imaging, Journal of Magnetic Resonance 190 (2008) 307–315.

[47] J. L. Yoder, P. E. Magnelind, M. A. Espy, M. T. Janicke: Exploring the limits of overhauser dynamic nuclear polarization (o-dnp) for portable magnetic resonance detection of low gamma nuclei, Applied Magnetic Resonance 49 (2018) 707–724.

[48] T. J. Keller, T. Maly: Overhauser dynamic nuclear polarization enhanced two-dimensional proton NMR spectroscopy at low magnetic fields, Magnetic Resonance (2021).

[49] S. Z. Kiss, N. MacKinnon, J. G. Korvink: Microfluidic overhauser DNP chip for signal-enhanced compact NMR, Scientific Reports 11 (2021).

[50] C. A. Fyfe, M. Cocivera, S. W. H. Damji: Flow and stopped-flow nuclear magnetic resonance investigations of intermediates in chemical reactions, Accounts of Chemical Research 11 (1978) 277–282.

[51] M. Godejohann, A. Preiss, C. Mügge: Quantitative measurements in continuous-flow HPLC/NMR, Analytical Chemistry 70 (1998) 590–595.

[52] M. Maiwald, H. H. Fischer, Y.-K. Kim, H. Hasse: Quantitative on-line high-resolution NMR spectroscopy in process engineering applications, Analytical and Bioanalytical Chemistry 375 (2003) 1111–1115.

[53] M. Maiwald, O. Steinhof, H. Hasse: Online-NMR-spektroskopie - mischungen messen im fluss, Nachrichten aus der Chemie 55 (2007) 745–749.

[54] R. Wei, A. M. R. Hall, R. Behrens, M. S. Pritchard, E. J. King, G. C. Lloyd-Jones: Stopped-flow 19f nmr spectroscopic analysis of a protodeboronation proceeding at the sub-second time-scale, European Journal of Organic Chemistry 2021 (2021) 2331–2342.

[55] C. G. Thomson, C. M. S. Jones, G. Rosair, D. Ellis, J. Marques-Hueso, A.-L. Lee, F. Vilela: Continuous-flow synthesis and application of polymer-supported BODIPY photosensitisers for the generation of singlet oxygen; process optimised by in-line NMR spectroscopy, Journal of Flow Chemistry 10 (2020) 327–345.

[56] K. H. Tsai, H. C. Dorn: A model for establishing the ultimate enhancements (a infinity) in the low to high magnetic field transfer dynamic nuclear polarization experiment, Applied Magnetic Resonance 1 (1990) 231–254.

[57] M. D. Lingwood, S. Han: Solution-state dynamic nuclear polarization, in: Annual Reports on NMR Spectroscopy, Elsevier, 2011, pp. 83–126.

[58] T. Cheng, M. Mishkovsky, M. J. N. Junk, K. Münnemann, A. Comment: Producing radical-free hyperpolarized perfusion agents for in vivo magnetic resonance using spin-labeled thermoresponsive hydrogel, Macromolecular Rapid Communications 37 (2016) 1074–1078.

[59] B. C. Dollmann, M. J. N. Junk, M. Drechsler, H. W. Spiess, D. Hinderberger, K. Münnemann: Thermoresponsive, spin-labeled hydrogels as separable DNP polarizing agents, Physical Chemistry Chemical Physics 12 (2010) 5879.

[60] M. D. Lingwood, A. J. Sederman, M. D. Mantle, L. F. Gladden, S. Han: Overhauser dynamic nuclear polarization amplification of nmr flow imaging, Journal of Magnetic Resonance 216 (2012) 94–100.

[61] R. Bahulekar, N. Ayyangar, S. Ponrathnam: Polyethyleneimine in immobilization of biocatalysts, Enzyme and Microbial Technology 13 (1991) 858–868.

[62] J. J. Virgen-Ortíz, J. C. S. dos Santos, Á. Berenguer-Murcia, O. Barbosa, R. C. Rodrigues, R. Fernandez-Lafuente: Polyethylenimine: a very useful ionic polymer in the design of immobilized enzyme biocatalysts, Journal of Materials Chemistry B 5 (2017) 7461–7490.

[63] R. R. de Melo, R. Alnoch, A. Sousa, H. H. Sato, R. Ruller, C. Mateo: Cross-linking with polyethylenimine confers better functional characteristics to an immobilized beta-glucosidase from exiguobacterium antarcticum b7, Catalysts 9 (2019) 223.

[64] M. A. Ghriga, B. Grassl, M. Gareche, M. Khodja, S. E. I. Lebouachera, N. Andreu, N. Drouiche: Review of recent advances in polyethylenimine crosslinked polymer gels used for conformance control applications, Polymer Bulletin 76 (2019) 6001–6029.

[65] A. W. Overhauser: Polarization of nuclei in metals, Physical Review 92 (1953) 411–415.

[66] C. P. Slichter: The discovery and renaissance of dynamic nuclear polarization, Reports on Progress in Physics 77 (2014) 072501.

[67] C. P. Slichter: The discovery and demonstration of dynamic nuclear polarization—a personal and historical account, Physical Chemistry Chemical Physics 12 (2010) 5741.

[68] A. Abragam, M. Goldman: Principles of dynamic nuclear polarisation, Reports on Progress in Physics 41 (1978) 395–467.

[69] M. Gafurov, V. Denysenkov, M. J. Prandolini, T. F. Prisner: Temperature dependence of the proton overhauser DNP enhancements on aqueous solutions of fremy's salt measured in a magnetic field of 9.2 t, Applied Magnetic Resonance 43 (2012) 119–128.

[70] D. Sezer, M. J. Prandolini, T. F. Prisner: Dynamic nuclear polarization coupling factors calculated from molecular dynamics simulations of a nitroxide radical in water, Physical Chemistry Chemical Physics 11 (2009) 6626.

[71] D. Sezer: Rationalizing overhauser DNP of nitroxide radicals in water through MD simulations, Phys. Chem. Chem. Phys. 16 (2014) 1022–1032.

[72] S. E. Küçük, P. Neugebauer, T. F. Prisner, D. Sezer: Molecular simulations for dynamic nuclear polarization in liquids: a case study of TEMPOL in acetone and DMSO, Physical Chemistry Chemical Physics 17 (2015) 6618–6628.

[73] C. Luchinat, G. Parigi: Nuclear relaxometry helps designing systems for solution DNP on proteins, Applied Magnetic Resonance 34 (2008).

[74] P. Neugebauer, J. G. Krummenacker, V. P. Denysenkov, C. Helmling, C. Luchinat, G. Parigi, T. F. Prisner: High-field liquid state NMR hyperpolarization: a combined DNP/NMRD approach, Phys. Chem. Chem. Phys. 16 (2014) 18781–18787.

[75] P. Höfer, G. Parigi, C. Luchinat, P. Carl, G. Guthausen, M. Reese, T. Carlomagno, C. Griesinger, M. Bennati: Field dependent dynamic nuclear polarization with radicals in aqueous solution, Journal of the American Chemical Society 130 (2008) 3254–3255.

[76] M. Bennati, C. Luchinat, G. Parigi, M.-T. Türke: Water 1h relaxation dispersion analysis on a nitroxide radical provides information on the maximal signal enhancement in overhauser dynamic nuclear polarization experiments, Physical Chemistry Chemical Physics 12 (2010) 5902.

[77] J. S. Hyde, J. C. W. Chien, J. H. Freed: Electron–electron double resonance of free radicals in solution, The Journal of Chemical Physics 48 (1968) 4211–4226.

[78] M.-T. Türke, M. Bennati: Saturation factor of nitroxide radicals in liquid DNP by pulsed ELDOR experiments, Physical Chemistry Chemical Physics 13 (2011) 3630.

[79] N. Enkin, G. Liu, M. del Carmen Gimenez-Lopez, K. Porfyrakis, I. Tkach, M. Bennati: A high saturation factor in overhauser DNP with nitroxide derivatives: the role of 14n nuclear spin relaxation, Physical Chemistry Chemical Physics 17 (2015) 11144–11149.

[80] R. A. Wind, J.-H. Ardenkjær-Larsen: 1h DNP at 1.4 t of water doped with a triarylmethyl-based radical, Journal of Magnetic Resonance 141 (1999) 347–354.

[81] P. Neugebauer, J. G. Krummenacker, V. P. Denysenkov, G. Parigi, C. Luchinat, T. F. Prisner: Liquid state DNP of water at 9.2 t: an experimental access to saturation, Physical Chemistry Chemical Physics 15 (2013) 6049.

[82] B. D. Armstrong, S. Han: Overhauser dynamic nuclear polarization to study local water dynamics, Journal of the American Chemical Society 131 (2009) 4641–4647.

[83] B. D. Armstrong, S. Han: A new model for overhauser enhanced nuclear magnetic resonance using nitroxide radicals, The Journal of Chemical Physics 127 (2007) 104508.

[84] C. E. Gallops, C. Yu, J. D. Ziebarth, Y. Wang: Effect of the protonation level and ionic strength on the structure of linear polyethyleneimine, ACS Omega 4 (2019) 7255–7264.

[85] I. Solomon: Relaxation processes in a system of two spins, Physical Review 99 (1955) 559–565.

[86] N. Bloembergen, L. O. Morgan: Proton relaxation times in paramagnetic solutions. effects of electron spin relaxation, The Journal of Chemical Physics 34 (1961) 842–850.

[87] A. Abragam: The Principles of Nuclear Magnetism, Clarendon Press, 1961.

[88] T. M. Carr, W. M. Ritchey: Toward an optimal paramagnetic relaxation agent for^{31}p NMR spectroscopy, Spectroscopy Letters 13 (1980) 603–633.

[89] N. Schork, M. Ibrahim, A. Baksi, S. Krämer, A. K. Powell, G. Guthausen: NMR relaxivities of paramagnetic, ultra-high spin heterometallic clusters within polyoxometalate matrix as a function of solvent and metal ion, ChemPhysChem 23 (2022).

[90] A. C. Venu, R. N. Din, T. Rudszuck, P. Picchetti, P. Chakraborty, A. K. Powell, S. Krämer, G. Guthausen, M. Ibrahim: NMR relaxivities of paramagnetic lanthanide-containing polyoxometalates, Molecules 26 (2021) 7481.

[91] P. Caravan, J. J. Ellison, T. J. McMurry, R. B. Lauffer: Gadolinium(III) chelates as MRI contrast agents: structure, dynamics, and applications, Chemical Reviews 99 (1999) 2293–2352.

[92] P. Caravan: Strategies for increasing the sensitivity of gadolinium based MRI contrast agents, Chemical Society Reviews 35 (2006) 512.

[93] A. M. R. Hall, J. C. Chouler, A. Codina, P. T. Gierth, J. P. Lowe, U. Hintermair: Practical aspects of real-time reaction monitoring using multi-nuclear high resolution FlowNMR spectroscopy, Catalysis Science & Technology 6 (2016) 8406–8417.

[94] H. H. Fischer, M. Seiler, T. S. Ertl, U. Eberhardinger, H. Bertagnolli, H. Schmitt-Willich, K. Albert: Quantification studies in continuous-flow ^{13}c nuclear magnetic resonance spectroscopy by use of immobilized paramagnetic relaxation agents, The Journal of Physical Chemistry B 107 (2003) 4879–4886.

[95] A. Bara-Estaún, M. C. Harder, C. L. Lyall, J. P. Lowe, E. Suturina, U. Hintermair: Paramagnetic relaxation agents for enhancing temporal resolution and sensitivity in multinuclear FlowNMR spectroscopy, Chemistry – A European Journal 29 (2023).

[96] R. Kircher, S. Mross, H. Hasse, K. Münnemann: Functionalized controlled porous glasses for producing radical-free hyperpolarized liquids by overhauser DNP, Molecules 27 (2022) 6402.

Appendix

A Supporting Information for High Flow-Rate Benchtop NMR Spectroscopy Enabled by Continuous Overhauser DNP

A.1 Electronic Equipment

Microwave sweep oscillator (8350B), frequency counter (5350A), as well as power meter (437B), equipped with a power sensor (8481B), were purchased from Hewlett Packard. The microwave amplifier was purchased from Varian (8-12 GHz, 20 W). The microwave equipment was basically identical with that used by Neudert et al.[45], who also gives additional information. The microwave resonator has to be cooled, as otherwise, the continuous microwave irradiation would lead to high temperatures in the microwave resonator. Cooling was accomplished by flushing the ENDOR probehead with cold nitrogen in a teflon sleeve in the Halbach magnet. The nitrogen was supplied by evaporating liquid nitrogen at ambient pressure. The temperature of the ENDOR probehead was measured by a platinum resistance thermometer and kept at about 288 K by adjusting the temperature of the nitrogen feed, which was controlled by electric heating. In principle, the ENDOR probehead can also be used to record NMR spectra, but due to the inhomogeneity of the magnetic field of the Halbach magnet and its low field strength, chemical shift and multiplicity information of components in mixtures is lost.

A.2 Magnetic Field Profile

The magnetic field profile in the equipment along the flow path is shown in Figure S1. Symbols represent measurements of the magnetic field at various positions of the setup with a Gaussmeter (GM08) manufactured from Hirst Magnetic Instruments Ltd. The outer boundaries of the Halbach magnet and housing of the benchtop NMR instrument are indicated by gray background. The measurement was started at the top of the Halbach magnet (position is 0 cm). The magnetic field of the Halbach magnet was adjusted to 0.35 Tesla and is homogeneous in the center at a distance of around 12 cm. The benchtop instrument was placed below the Halbach magnet, see Figure 1. The distance between the microwave cavity of the ENDOR probehead that is positioned in the Halbach magnet and the RF coil of the benchtop NMR spectrometer is about 0.5 m.

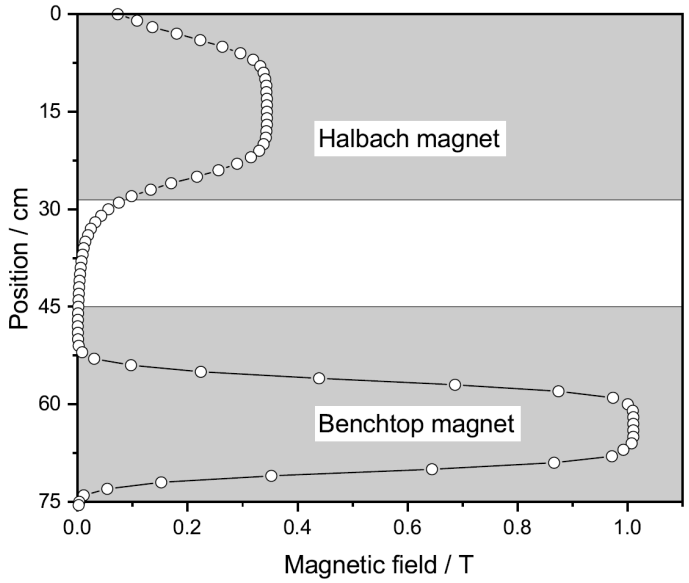

Figure S1: Magnetic field profile of the experimental setup used in the present work. Symbols represent measurements of the magnetic field at various positions of the setup. The outer boundaries of the Halbach magnet and housing of the benchtop NMR instrument are indicated by gray background. Solid line: guide the eye.

B Supporting Information for Functionalized Controlled Porous Glasses for Producing Radical-Free Hyperpolarized Liquids by Overhauser DNP

B.1 Synthesis of CPG Radical Matrices

The chemicals used in the following synthesis are listed in Table B1. Two syntheses are presented, which provide different couplings to the support material: (1) without additional linker; (2) with PEI- and BDGE-linker.

(1) Aminopropyl-CPGs (350 mg) were added to ethanol (5×2 mL) and centrifuged in each case (5 min at 2500 rpm). The supernatant was removed. 4-Glycidyloxy-2,2,6,6-tetramethylpiperidinyloxyl (GT, 399.56 mg, 0.5 mM) was dissolved in methanol. This radical solution was added to previously prepared CPGs and the reaction mixture was rotated in a tube rotator for 24 h at room temperature. Water (5×15 mL) was added and CPGs were separated by filtration . The product was stored in water (2.0 mL) at 277 K.

(2) Aminopropyl-CPGs (350 mg) were added to ethanol (5×2 mL) and centrifuged in each case (5 min at 2500 rpm). The supernatant was removed. BDGE (283.15 mg) was dissolved in methanol (3.5 mL) and dry aminopropyl-CPGs were added. The reaction mixture was rotated in a tube rotator for 24 h at room temperature. Water (5×15 mL) as well as ethanol (2×15 mL) was added and centrifuged in each case (5 min at 2500 rpm). Polyethyleneimine (molecular mass of 800 g mol^{-1}, 280 mg, 100 mM; molecular mass of 25.000 g mol^{-1}, 8.75 g, 20 mM) was dissolved in methanol and the previously BDGE-grafted CPGs were added. The reaction mixture was rotated in a tube rotator for 24 h at room temperature. Water (5×15 mL) as well as afterwards ethanol (2×15 mL) was added and centrifuged in each case (5 min at 2500 rpm). Finally, GT (399.56 mg, 0.5 mM) was dissolved in methanol. This radical solution was added to prepared PEI-grafted CPGs and the reaction mixture was rotated in a tube rotator for 24 h at room temperature. Water (5×15 mL) was added and CPGs were separated by filtration. The product was stored in water (2.0 mL) at 277 K.

Table B1: Chemicals used in the presented immobilization procedure of GT onto aminopropyl-functionalized CPGs are listed with the respective suppliers and purities.

Chemical	Supplier	Purity
Aminopropyl-CPGs	Biosearch Technologies	
GT	TCI	> 0.95 g g^{-1}
Polyethyleneimine 25000 g mol^{-1}	Sigma Aldrich	> 0.99 g g^{-1}
Polyethyleneimine 800 g mol^{-1}		> 0.98 g g^{-1}
1,4-Butanediol diglycidyl ether		> 0.95 g g^{-1}
Methanol		> 0.99 g g^{-1}
Ethanol		> 0.99 g g^{-1}
Acetonitrile		> 0.99 g g^{-1}

B.2 Experimental Procedures

B.2.1 EPR Measurements

A MicroESR-X-Band spectrometer from Bruker was used to determine the radical loading of synthesized CPG radical matrices. EPR measurements were performed using microcapillaries from Blaubrand intramark and were sealed with Leica Microsystems Critoseal capillary tube sealant. Sample volume was around 4 µL. The radical matrix was previously stored in a large supernatant (20 mL) of acetonitrile or water for 24 h. The entire sample volume was filled with the radical matrix in static contact with the liquid to be investigated and the supernatant was removed carefully. The following parameters are used: microwave power 15 mW, modulation coil amplitude 1.0 G, receiver gain 12 dB and an average of 16 scans was used. The relative error in the results of our EPR measurements is less than 2%. The accuracy in quantification of GT with the obtained calibration line of dissolved GT in water, is around 97%. The relative error of presented immobilized GT concentration values is around 3%.

B.2.2 Inversion Recovery NMR Measurements

^{1}H NMR measurements were performed using a 1 Tesla benchtop NMR spectrometer (Spinsolve carbon, proton frequency of 43 MHz) manufactured by Magritek. 2.5 mm outer diameter special microprobe NMR tubes from Norell were used to minimize the

sample volume. After the liquid and radical matrix to be examined was transferred into the NMR tubes, the supernatant was removed after brief centrifugation. Parameters of the inversion recovery measurements were set with the standard protocol supplied by Magritek, taking care that the delay between the individual measurements was chosen sufficiently high for complete equilibration of the nuclear spins, as well as the maximum inversion time. An averaging of 8 scans was used. The relative error in successive T_1 measurements is less than 1% in this work.

B.2.3 Static ODNP Measurements

Hyperpolarization is always generated with an ENDOR probehead (EN4148X-MD4) from Bruker at 0.35 Tesla in the Halbach magnet. The same microcapillaries as described for the EPR measurements were used and the sample preparation is carried out similarly. Samples for ODNP measurements with varying pH are prepared using a 0.2 M hydrochloric acid solution and ultrapure water (produced in our laboratory with an Elix Essential 5 purification system from Merck Millipore). Dilution and also the pH measurement were performed with an 848 Titrino plus system from Metrohm. All measurements presented here were performed five times, with preparation of a new sample each time. The following parameters were used: microwave frequency was 9.67 GHz, microwave power was adjusted in a range between 0.5 and 2.5 W and single-scan acquisition. An average of 16 scans was used for the thermally polarized NMR measurements. Samples were irradiated for period of about five times the T_1^{RM} of the liquid in static contact with the CPG radical matrices. In ODNP measurements with varying pH the microwave power was adjusted to 6 W. Static enhancements were calculated using the integral of the hyperpolarized signal (microwave on) divided by the integral of the thermally polarized signal (microwave off) that were measured directly in the ENDOR probehead.

B.2.4 Flow ODNP Measurements

NMR data were always acquired with the 1 Tesla benchtop NMR spectrometer in flow mode. NMR measurements are acquired with short acquisition times of around 400 ms. The delay between individual NMR scans was set to 2 s, which was used to ensure a full exchange of the liquid in the active volume of the RF coil even at low flow-rates. All measurements presented here were performed three times. The following parameters were used: microwave frequency was 9.67 GHz, microwave power was adjusted in a range between 0.5 and 6.1 W and single-scan acquisition. An average of 16 scans was used for the thermally polarized NMR measurements. An HPLC pump manufactured

by Flusys was used to set up the liquid flow, which is equipped with a mass flow meter (Mini CORI-Flow) purchased from Bronkhorst. Hyperpolarization is generated in the ENDOR probehead in the 0.35 Tesla Halbach magnet in the first part of the set-up. Flow enhancements were calculated using the integral of the hyperpolarized signal (microwave on) divided by the integral of the thermally polarized signal (microwave off) that were measured in the benchtop NMR spectrometer.

B.3 Quantification of Radicals by EPR Spectroscopy

EPR spectra were recorded with a MicroESR-X-Band spectrometer from Bruker. EPR spectra of dissolved 4-glycidyloxy-2,2,6,6-tetramethylpiperidine-1-oxyl (GT) in water are shown in Figure S2. Integrals of absorption spectra were used to generate a calibration line (y=a+b*x; $R^2 = 0.97$; see Figure S3) that was used to calculate the amount of immobilized GT of synthesized CPG radical matrices. EPR measurements were performed using microcapillaries from Blaubrand intramark with an inner diameter of 1 mm with a sample volume of 4 µL and were sealed with Leica Microsystems Critoseal capillary tube sealant. The following EPR acquisition parameters were used: microwave power 15 mW, modulation coil amplitude 1.0 G, receiver gain 12 dB and an average of 16 scans. This set of EPR parameters was also used in all following EPR measurements of synthesized CPGs in order to allow the quantitative evaluation of radical concentrations. The parameters are adjusted to higher concentrations of GT and thus, digitalization noise is visible for small concentrations of immobilized GT of radical matrices of the type CPG-PEI800-GT.

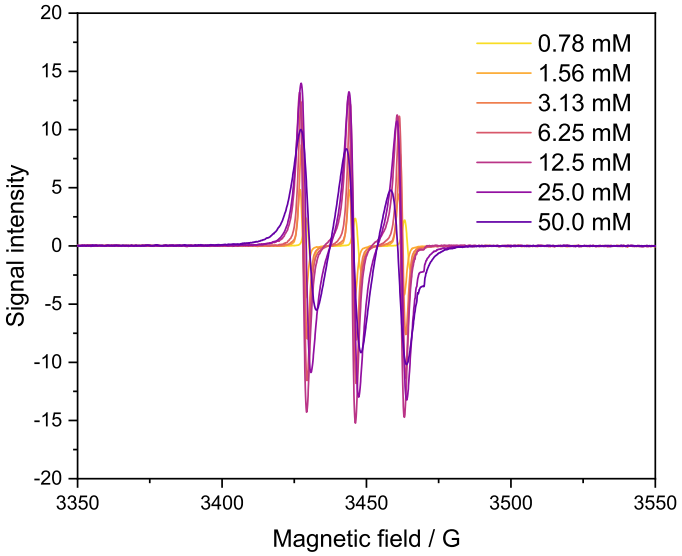

Figure S2: Results from EPR measurements of dissolved GT in the concentration range of 1 mM to 50 mM in water.

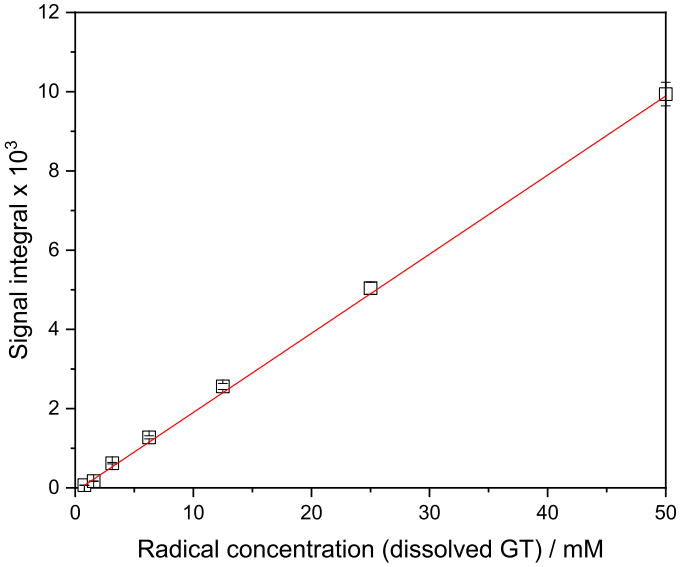

Figure S3: Calibration line from EPR measurements of dissolved GT (shown in Figure S2) in the concentration range of 1 mM to 50 mM in water.

To study the amount of immobilized GT of synthesized radical matrices, 100 mg of each radical matrix was previously stored in a large supernatant (20 mL) of acetonitrile or water for 24 h. The entire sample volume of 4 µL was filled with the radical matrix in static contact with the liquid to be investigated and the supernatant was removed carefully after brief centrifugation.

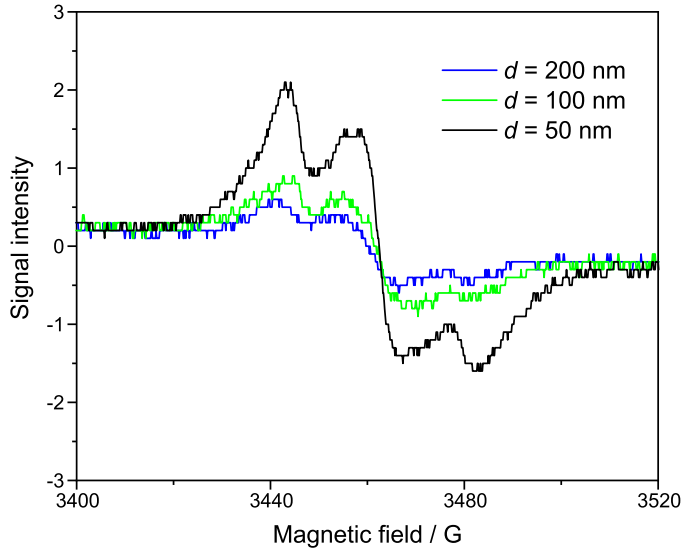

Figure S4: Results from EPR measurements of the synthesized CPGs of the type CPG-PEI800-GT with different pore size d in water.

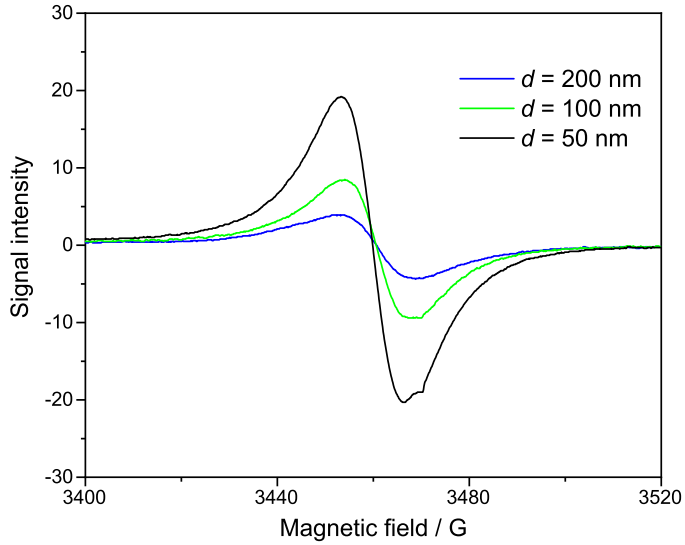

Figure S5: Results from EPR measurements of the synthesized CPGs of the type CPG-PEI25000-GT with different pore size d in water.

Figure S4 and Figure S5 show the first derivative of the EPR spectra of synthesized CPG radical matrices with different pore sizes of 50, 100, and 200 nm with the coupled polyethyleneimine (PEI) polymer PEI800 and PEI25000 in water. The amount of immobilized GT was calculated by comparison of EPR integrals with aqueous solutions of GT of known concentrations, see Figure S3 and calculated concentration values are listed in Table 2. The immobilization of GT leads to a significant broadening of the measured EPR lines. This effect combined with Heisenberg spin exchange at high radical loading accomplished with the high molecular weight polymer results in a single broad line for radical matrices of the type CPG-PEI25000-GT in the absorption spectrum.

B.4 Leakage Factors with Dissolved TEMPO-Radicals

Leakage factors were calculated using Equation 3. This ODNP parameter was directly accessible via NMR inversion recovery measurements that were performed with a 1 Tesla benchtop NMR spectrometer from Magritek. 2.5 mm outer diameter special microprobe NMR tubes from Norell were used to minimize the sample volume. Parameters of the inversion recovery measurements were set with the standard protocol supplied by Magritek, taking care that the delay between the individual measurements was chosen sufficiently high for complete equilibration of the nuclear spins, as well as the maximum inversion time. An average of 8 scans was used.

T_1 values of acetonitrile and water in static contact with dissolved TEMPO radicals are shown in Figure S6. In this work, a specially functionalized TEMPO radical was used, namely 4-glycidyloxy-2,2,6,6-tetramethylpiperidine-1-oxyl (GT). The relaxation behavior of acetonitrile and water was studied, which were doped with dissolved 4-hydroxy-TEMPO (HT), 4-amino-TEMPO (AT), and GT of different concentrations.

The relaxation efficiency for water and acetonitrile does not change with the different functionalization of TEMPO, as expected, because the functionalization is far from the unpaired electron delocalized via the N-O bond, which is additionally shielded by the neighboring methyl groups. Figure S7 shows calculated leakage factors in dependence of the radical concentration of dissolved TEMPO radicals in acetonitrile and water. For the relaxation behavior of acetonitrile and water with dissolved TEMPO-radicals, the leakage factor is always better for water than for acetonitrile at a comparable concentration of TEMPO, which points to a preferred radical-target molecule interaction with water.

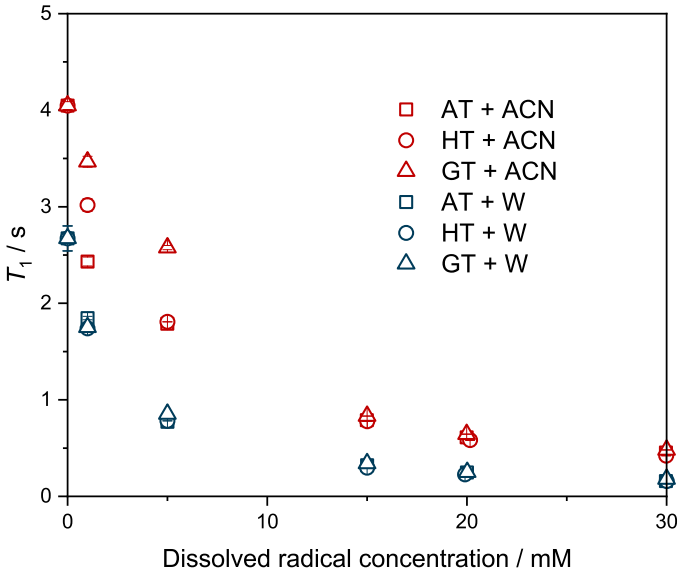

Figure S6: Results of inversion recovery measurements with water (W) and acetonitrile (ACN) in contact with dissolved TEMPO radicals, i.e. 4-amino-TEMPO (AT), 4-hydroxy-TEMPO (HT) and 4-glycidyloxy-TEMPO (GT). The symbols are experimental results and were obtained as the arithmetic mean of three individual samples. The error bars indicate the standard deviation.

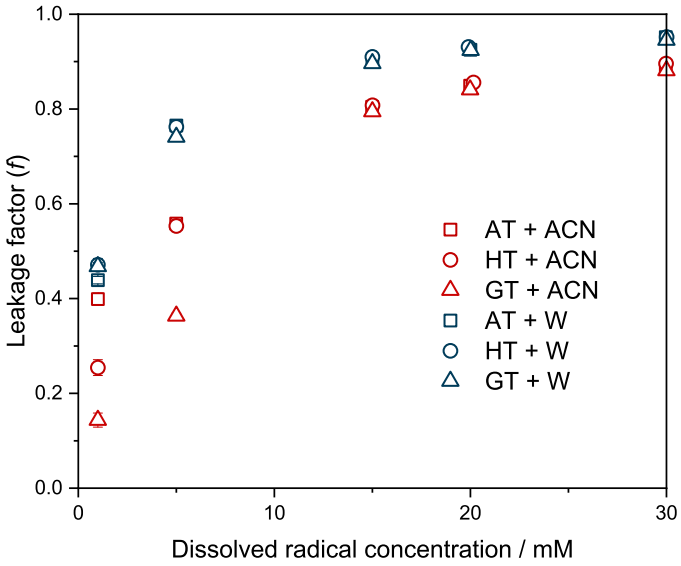

Figure S7: Results of calculated ODNP leakage factors with water (W) and acetonitrile (ACN) in contact with dissolved TEMPO radicals, i.e. 4-amino-TEMPO (AT), 4-hydroxy-TEMPO (HT) and 4-glycidyloxy-TEMPO (GT). The symbols are experimental results and were obtained as the arithmetic mean of three individual samples. The error bars indicate the standard deviation. Leakage factors are calculated with Equation 3.

B.5 Leakage Factors with CPG Radical Matrices

Sample preparation and NMR acquisition was carried out similarly to the experiments with dissolved radicals. After the liquid and radical matrix to be examined was transferred into the NMR tubes, the supernatant was removed after brief centrifugation. Figure S8 shows calculated leakage factors in dependence of the radical concentration of CPG radical matrices in acetonitrile and water, the corresponding T_1 values are listed in Table 3. The behavior of the leakage factor is influenced purely by the immobilized radical loading in the CPG radical matrices and no further effect of the pore size can be seen in the range of CPG pore diameters studied here.

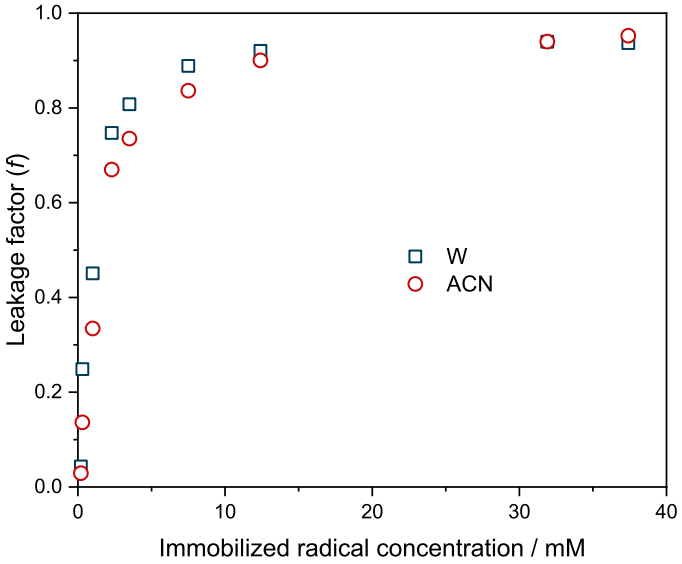

Figure S8: Results of calculated ODNP leakage factors versus radical concentration of synthesized CPG radical matrices in pure water (W) and acetonitrile (ACN). Leakage factors are calculated with T_1 values listed in Table 3 and Equation 3.

B.6 Flow ODNP of Acetonitrile

Figure S9 shows results of continuous ODNP measurements with CPG-PEI25000-GT (pore size 50 nm) with acetonitrile, in which both the microwave power and the flow-rate were varied. The highest flow-rate corresponds to a superficial flow velocity of about 0.7 m s^{-1}. From ODNP data dependent on microwave power, E_{max}^{flow} values for the enhancement at infinite microwave power can be extracted by exponential extrapolation [31, 82]. Figure S9 demonstrates that a large sensitivity improvement in continuous-flow benchtop NMR spectroscopy can be accomplished by ODNP also for acetonitrile. This is especially important in the fast flow-regime where the thermal NMR signal almost completely vanishes due to very short prepolarization times.

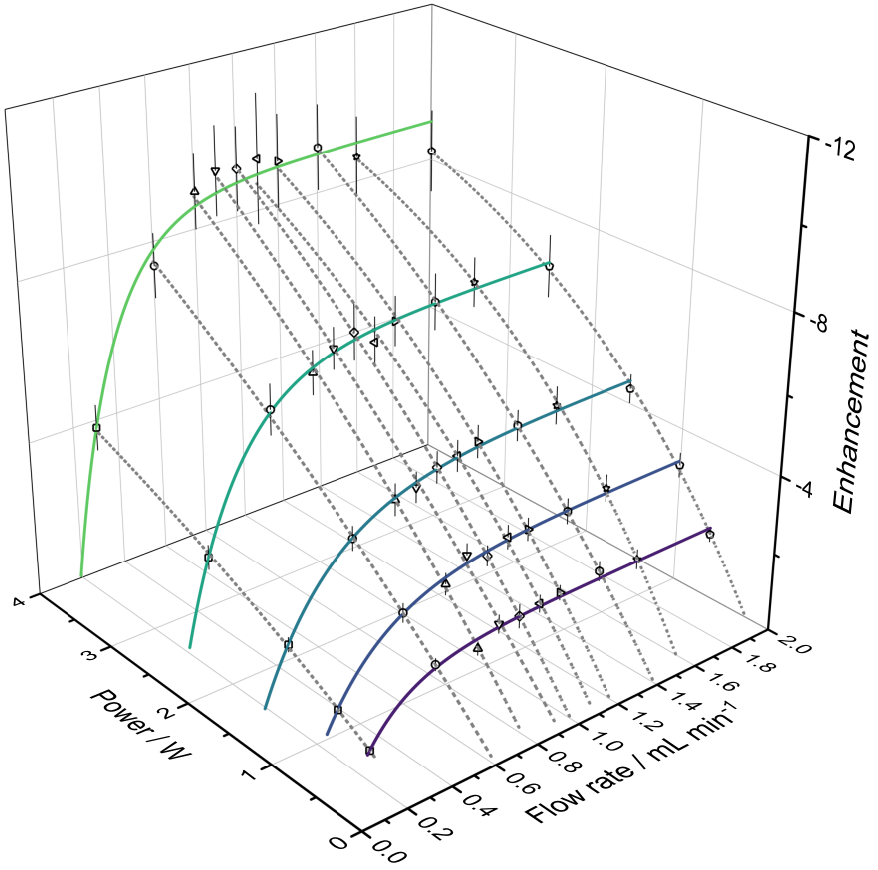

Figure S9: Results from continuous-flow ODNP measurements with acetonitrile obtained with CPG-PEI25000-GT (pore size 50 nm) versus applied microwave power and flow-rate. The symbols are experimental results and were obtained as the arithmetic mean of the results of three individual samples. Solid lines: guide to the eye. Dashed lines: exponential fit [31, 82].

Declaration

This cumulative dissertation contains material that has been published previously or that is included in submitted publications. In the following, these publications are listed together with a statement on the contributions of the author of the present dissertation.

- R. Kircher, H. Hasse, K. Münnemann: High Flow-Rate Benchtop NMR Spectroscopy Enabled by Continuous Overhauser DNP, Analytical Chemistry 93, 25 (2021) 8897-8905,
  DOI: 10.1021/acs.analchem.1c01118.

  The author designed and constructed the experimental set-ups, synthesized the ODNP radical matrix, performed NMR measurements, and wrote the manuscript.

- R. Kircher, S. Mross, H. Hasse, K. Münnemann: Functionalized Controlled Porous Glasses for Producing Radical-Free Hyperpolarized Liquids by Overhauser DNP, Molecules 27, 19 (2022) 6402,
  DOI: 10.3390/molecules27196402.

  The author built the set-up, designed the ODNP radical matrix, performed NMR measurements, and wrote the manuscript.

- R. Kircher, S. Mross, H. Hasse, K. Münnemann: Quantitative Analysis in Continuous-Flow ^{1}H Benchtop NMR Spectroscopy by Paramagnetic Relaxation Enhancement
  DOI: 10.1007/s00723-023-01626-8.

  The author built the set-up, designed the PRE agent, performed PRE-enhanced benchtop NMR measurements, and wrote the manuscript.

Student Theses

The following student theses were prepared under the supervision of the author of the present doctoral thesis in the frame of his research:

- K. Malinovska: Synthesis of Functionalized 2,2,6,6-Tetramethylpiperidinyloxyl Carrier Materials for DNP-Enhanced NMR Spectroscopy. Student thesis, Laboratory of Engineering Thermodynamics (LTD), TU Kaiserslautern (2018).
- K. Maurer: Agenzien zur Herabsetzung der T_1-Zeit für die Verbesserung von NMR Flussexperimenten. Student thesis, LTD, TU Kaiserslautern (2019).
- K. Malinovska: Synthesis of Radical Support Materials for DNP-enhanced NMR Spectroscopy. Master thesis, LTD, TU Kaiserslautern (2019).
- F. Möhler: CFD Simulation von Systemen zur DNP-verstärkten quantitativen NMR-Analytik im Fluss. Master thesis, LTD, TU Kaiserslautern (2019).
- S. Mross: Synthesis of Radical Matrices for DNP NMR Spectroscopy in Continuous Flow. Master thesis, LTD, TU Kaiserslautern (2020).

Curriculum Vitae

Name:	Raphael Kircher
Place of birth:	Speyer
Nationality:	German

Education

1999 – 2003	Elementary school in Lachen-Speyerdorf
2003 – 2004	Secondary school in Hassloch
2004 – 2012	Hannah-Arendt-Gymnasium in Hassloch
	Degree: Allgemeine Hochschulreife
2012 – 2017	Studium at TU Kaiserslautern
	Program: Diplom Chemie
	Degree: Dipl.-Chem.

Professional

08/2017 – 03/2022	PhD student at the Laboratory of Engineering Thermodynamics
	TU Kaiserslautern
	Prof. Dr.-Ing. Hans Hasse
04/2022 – 11/2023	Scientist at the Helmholtz-Institut Mainz
	GSI Helmholtzzentrum für Schwerionenforschung Darmstadt
	Johannes-Gutenberg University Mainz
	Prof. Dr. Dmitry Budker